Breakdown of cooperative architecture in multispecies biofilms and the spatial ecology of predation

Benjamin R. Wucher[1], Mennat Elsayed[2], Daniel E. Kadouri[2], Carey D. Nadell[1]*

[1] Department of Biological Sciences, Dartmouth, 78 College St., Hanover, NH 03755, USA
[2] Department of Oral Biology, Rutgers School of Dental Medicine, 110 Bergen St., Newark, NJ 07101, USA

*Author for correspondence:
Carey D. Nadell (ORCID: 0000-0003-1751-4895)
1978 Life Sciences Center
78 College St., Hanover NH 03755
Email: carey.d.nadell@dartmouth.edu
Phone: 603-646-1525

Abstract

Adherence to surfaces and secretion of extracellular matrix, or biofilm formation, is common in the microbial world, but we often do not know how ecological interaction at the cellular spatial scale translates to biofilm community ecology. Here we explore an especially understudied element of biofilm ecology, namely predation by the bacterium *Bdellovibrio bacteriovorus*. This predator can kill and consume many different Gram-negative bacteria, including *Vibrio cholerae* and *Escherichia coli*. *V. cholerae* can protect itself from predation within highly packed biofilm structures that it creates, whereas *E. coli* biofilms are generally highly susceptible to *B. bacteriovorus*. Here we explore how predator-prey dynamics are altered when *V. cholerae* and *E. coli* are growing in biofilms together. We find that in dual species prey biofilms, *E. coli* predation survival increases, whereas *V. cholerae* survival decreases. *E. coli* benefits from predator protection when they become embedded within expanding groups of highly packed *V. cholerae*. But we find, interestingly, that normal, ordered and highly packed biofilm structure of *V. cholerae* can be disrupted if *V. cholerae* cells are directly adjacent to *E. coli* cells at the start of biofilm growth. When this occurs, the two species become entangled, and the resulting disordered cell groups do not block predator entry. Because biofilm cell group structure depends on initial cell distributions at the start of prey biofilm growth, the colonization dynamics have a dramatic impact on the eventual multispecies biofilm architecture, which in turn determines to what extent both species survive exposure to *B. bacteriovorus*.

Significance

Bacteria live in multispecies, spatially structured communities ubiquitously in the natural world. These communities, or biofilms, have a strong impact on microbial ecology, but we often do not know how cellular scale interactions determine overall biofilm structure and community dynamics. Here we explore this problem in the context of predator-prey interaction, with two prey species – *Vibrio cholerae* and *Escherichia coli* – being attacked by the bacterial predator *Bdellovibrio bacteriovorus*. We find that when *V. cholerae* and *E. coli* grow together in biofilms, the architectures that they both produce change in ways that cannot be predicted from looking at each prey species alone, and that these changes in cell group structure crucially impact the community dynamics of predator-prey interaction in biofilms.

Introduction

Most organisms do not naturally live in isolated monocultures but rather in communities composed of many species, and microbes are no exception [1–4]. Bacterial communities are present ubiquitously including sinking detritus particles in aquatic environments, deep-sea hydrothermal vents, rhizosphere habitats, animal digestive tracts, plant roots and shoots, fouling surfaces across human industry, and many types of chronic infections [5–19]. In many of these contexts, surface attachment and growth in large cell groups, or biofilm formation, are important strategies for sequestering limited space and nutrients, as well as protecting against common biotic and abiotic threats [20–25]. Biofilms are small scale ecosystems encased in a wide range of secreted polymeric substances that control cell-cell and cell-surface engagement[26–32]. The benefits of biofilm formation have been examined in many contexts, showing their capacity for public goods sequestration, exclusion of newly arriving competitors, predation protection, and antibiotic tolerance[33–37]. The precise costs and benefits of biofilm formation vary across species, as do the multicellular architectures that emerge from the combination of cell growth, matrix secretion, and environmental feedbacks[23,27,29,38–46]. In what few cases have been examined, multispecies biofilms create structures that may be distinct from those found in single species biofilms of the community constituents in isolation[47–49]. Understanding the connections between biofilm architecture and microbial community ecology at different scales remains an important area for ongoing work on numerous topics, including cross-feeding relationships, diffusible and contact-mediated toxin antagonism, resilience against antibiotics in therapeutic contexts, industrial and medical surface degradation, and others[50–56].

Predation within biofilms is a broad sub-class of microbial ecology that has received relatively little attention with high resolution imaging and analysis. While many predators, such as phages, can usually attack only a small number of prey species, the ubiquitous predator *Bdellovibrio bacteriovorus* can be considered a generalist[36,57–60]. It is not known to rely on a specific receptor for cell entry and can prey on a wide variety of proteobacteria[8,59,61–63]. However, the extent of its predation on biofilm-dwelling target cells appears to vary widely between prey species, and the mechanisms underlying this variability remain mostly unknown.

Studies using macroscopic measurement techniques have reported the susceptibility of several biofilm-producing species to *B. bacteriovorus* predation[57]. For example, *Escherichia coli* and *Pseudomonas fluorescens* can be reduced to non-detectable levels by *B. bacteriovorus* in laboratory biofilm culture[36]. We recently documented a different outcome in *Vibrio cholerae* biofilms, which can protect themselves from predator exposure via their highly packed cell arrangements that occur after the prey cell groups grow beyond several hundred cells[35]. Given that we have examples of prey species whose biofilm structure protects them from *B. bacteriovorus* predation, and other prey whose biofilms confer little or no protection at all, we were curious as to what would happen to predator-prey dynamics in multi-species prey biofilm contexts. How often and to what extent does the cellular architecture of the two species depart from what is normally observed in monoculture? How do any of these changes influence the susceptibility of different prey species to *Bdellovibrio* predation, and overall predator-prey population dynamics?

We chose two proteobacteria – *V. cholerae* and *E. coli* – to study these questions. Both species have been isolated from biofilms in the same environments in proximity to humans, and they have been documented to co-infect hosts[64–69]. Their respective biofilm formation mechanics have also been very well characterized. *V. cholerae* forms dense, tightly packed cell groups with radially aligned cell arrangements, whose structure depends on the matrix proteins RbmA, RbmC, and Bap1, as well as VPS, its core exopolysaccharide[27,28,40,70–72]. This highly packed cell group architecture is critical for protection from phages and *B. bacteriovorus* attack[35,37] . The cell packing required for predator protection does not occur immediately as biofilm growth begins, though, leaving nascent *V. cholerae* cell groups open to predation. *E. coli* in contrast forms its biofilms with many different matrix components including cellulose, polyglycolic acid, colanic acid, Type 1 fimbriae, flagellar filaments, and curli fiber proteins[73]. *E. coli* matrix

architecture, and curli protein in particular, have been shown to confer protection against phage exposure, but other prior work has indicated even structurally mature *E. coli* biofilms are not protected from *B. bacteriovorus*[57,74]. Here we use single cell resolution microscopy to examine the structure of these two prey species in monoculture and dual-culture biofilms, finding that the multispecies context causes unexpected changes in biofilm architecture that in turn alter predator-prey interaction and the overall population dynamics.

Results

Predation in dual-species prey biofilms has inverse fitness effects for *V. cholerae* and *E. coli*

We engineered *V. cholerae* N16961, *E. coli* AR3110, and *B. bacteriovorus* 109J to constitutively produce the fluorescent proteins mKate2, mKO-κ, and mGFP, respectively, so that they could be distinguished for live confocal microscopy. The N16961 parental strain of *V. cholerae* is repressed for Type 6 Secretion System activity in laboratory culture conditions, and so does not kill *E. coli* via this mechanism in our experiments[75,76]. Overnight cultures of the two prey species were diluted and re-grown to mid-exponential phase (OD_{600} = 0.5-0.7) before inoculating them at a 1:1 ratio into poly-dimethylxilosane microfluidic flow devices bonded to coverslip glass (see Methods). In parallel we performed mono-culture experiments in which *V. cholerae* and *E. coli* were introduced to chambers on their own. Cells were allowed to colonize the underlying glass surface in stationary conditions for 1 h, after which M9 minimal media with 0.5% glucose was introduced into the chambers at 0.2 μL/min (average flow velocity = 90 μm/s). After 48 h of growth in co-culture, groups with varying composition of both species could be found distributed throughout the chambers (SI Figure S1A), and prior to exposure to *B. bacteriovorus*, the two prey species equilibrated at frequencies of approximately 80% *V. cholerae* and 20% *E. coli* (Figure 1A; SI Figure S1A). Following 48 h of prey biofilm growth, we introduced *B. bacteriovorus* under continuous flow for 1h, followed by a return to influx of sterile M9 media for both the dual culture chambers and the monoculture controls. When exposed to *B. bacteriovorus* in a mono-species context, *V. cholerae* survives within cell groups that have reached high cell packing (biovolume fractions of 0.8 and higher), as we have shown previously[35]. 48 h following predator exposure, monoculture *V. cholerae* biofilms maintain net positive growth (Figure 1A, B). By contrast, and consistent with prior reports, *E. coli* biofilms in monoculture exhibit little to no survival in the presence of *B. bacteriovorus*, with prey biomass falling below detectable levels 48 h after predator introduction (Figure 1A,B; SI Figure S1B)[36].

If *B. bacteriovorus* predates *V. cholerae* and *E. coli* independently of one another in dual prey species biofilms, we would expect residual *V. cholerae* biomass and elimination of all *E. coli* subpopulations, as seen in the prey monoculture experiments above. However, examining the population dynamics quantitatively, we found a significant increase in *E. coli* survival and a significant decrease in *V. cholerae* survival following predator introduction in the dual-species condition relative to the single species controls (Figure 1A,B). These results imply nonlinear interactions between *V. cholerae*, *E. coli*, and *B. bacteriovorus*, which alter prey population dynamics in a manner that the prey mono-species controls cannot predict. Below we explore why *E. coli* fares better in dual-species biofilms against predator exposure, and why *V. cholerae* fares worse, relative to their respective single species prey conditions.

E. coli gains protection from predator exposure while embedded within *V. cholerae* cell groups

Prior to introduction *of B. bacteriovorus* predators, we noticed that the spatial distributions of *V. cholerae* and *E. coli* in dual-culture prey biofilms were heterogeneous on scales of 10-100 μm, and in many instances, there were groups of *E. coli* cells that had been enveloped by expanding colonies of highly packed *V. cholerae*. 48 h following introduction of predators, virtually all surviving *E. coli* were those embedded within packed *V. cholerae* biofilms in this manner (Figure 2A; Figure S2). As previously documented, *V. cholerae* biofilm clusters reach a cell packing threshold that blocks predator entry and allows the interior cells to survive[35]. *E. coli* enveloped within *V. cholerae* groups that have reached this threshold appear to gain the predation protection conferred by *V. cholerae* biofilm structure. To assess this point in more detail we quantified the extent of *E. coli* predation and *V. cholerae* fluorescence in proximity to *E. coli* in these images, and these two measures were clearly anti-correlated in space (Figure 2B,C). Furthermore, protection of *E. coli* within *V. cholerae* cell groups was dependent on the high-density structure that wild type *V. cholerae* creates. When the experiment was repeated with a mutant strain of *V. cholerae* that cannot produce RbmA – a matrix component required for the tight cell packing found in mature biofilms – *B. bacteriovorus* could freely enter and access both *V. cholerae* and *E. coli* (SI Fig S3A,B). In this case, almost all cells of both species were killed off by the predators (SI Figure S3C,D). In a parallel study, we show that all of these results are replicated if virulent lytic or temperate phages targeting *E. coli* are introduced to biofilms of *E. coli* and *V. cholerae* grown in co-culture (Winans et al., 2022, *bioRxiv*)[77].

Although *E. coli* cells embedded within *V. cholerae* biofilms gain predator protection, it was not clear if they remain viable, or if they are able to subsequently disperse to colonize downstream locations. If not, then the protection *E. coli* gains from *B. bacteriovorus* exposure within *V. cholerae* cell groups would not necessarily translate to meaningful fitness gains on longer time scales. We explored this question by inducing dispersal with an increased flow rate (see Methods) and allowing the two species to colonize new microfluidic devices connected downstream from the initial chamber. In this new downstream chamber, both species could be found attached and replicating. This outcome demonstrates that the protected inclusions of *E. coli* cells within *V. cholerae* biofilms are viable and can successfully disperse to colonize new spaces (SI Figure S4).

The predation protection gained by *E. coli* cell groups embedded within highly packed *V. cholerae* biofilm clusters explains the increase in *E. coli* survivorship that we originally observed in dual culture. We note however that the *V. cholerae* cells within these highly packed cell groups are also protected from *B. bacteriovorus* predation, so the results so far do not yet explain why *V. cholerae* survivorship declines in co-culture with *E. coli* under predation pressure.

<u>Co-culture with *E. coli* can lead to breakdown of *V. cholerae* biofilm architecture</u>

In the previous section we made note of highly packed *V. cholerae* biofilms into which *E. coli* had become embedded and gained protection from *B. bacteriovorus* exposure. These colonies appear to behave in much the same way as mono-species *V. cholerae* biofilms, as they contain large continuous groups of *V. cholerae* in their ordered radial alignment and tight packing, albeit with pockets of *E. coli* included as well (Figure 3A, B). This growth pattern was not the only kind that emerged in prey co-culture experiments, however: there was a second, qualitatively distinct colony architecture in which *V. cholerae* and *E. coli* were homogenously mixed together (Figure 3A, C). These colonies were disordered in comparison with the radial alignment in ordered *V. cholerae* cell groups, with visibly reduced cell packing density. *B. bacteriovorus*

could enter throughout these disordered cell groups, gaining access to and killing most or all *V. cholerae* and *E. coli* cells within them (Figure 3A,C).

To study the differences between the ordered and disordered colony structure in more detail, we isolated examples of each for further analysis (Figure 3B,C). The relative abundance of *V. cholerae* looked to be somewhat lower in disordered colonies (Figure 3B,C, see also next section for quantitative detail). The combined cell packing of the two species together was indeed diminished in disordered colonies (Figure 3D), falling below the threshold (biovolume fraction ~0.8) necessary for predation protection in ordered *V. cholerae* colonies[35]. An alternative but not mutually exclusive factor for predation susceptibility for *V. cholerae* could be abundance of *E. coli* in their immediate vicinity. However, measurements of the relationship between *V. cholerae* predation and local abundance of *E. coli* in the two colony types clearly shows that overall colony structure is the dominant factor controlling the extent of predation by *B. bacteriovorus* (Figure 3E). A similar reciprocal analysis of *E. coli* predation as a function of colony type and local abundance of *V. cholerae* gave the same outcome (Figure S5). The shift in architecture between ordered and disordered cell groups also appeared to be driven entirely by the loss of *V. cholerae*'s ability to produce highly packed clusters, as it normally does on its own. Examining the cell packing of groups formed after 48 h supports this interpretation, as *V. cholerae* within-species cell packing with respect to itself (in contrast with combined cell packing of the two species together noted in (Figure 3D) shifted dramatically between ordered versus disordered biofilm types (Figure 3F,G). *E. coli* within-species cell packing, on the other hand, was the same in ordered versus disordered cell groups (Figure 3F,H).

Our results thus far indicate that in mixed prey biofilms of *V. cholerae* and *E. coli*, a fraction of the *E. coli* becomes engulfed within *V. cholerae* cell groups with ordered high packing structure that protects both species from *B. bacteriovorus*. This observation explains the improvement in *E. coli* predation survival in dual culture relative to monoculture biofilms. On the other hand, a fraction of the *V. cholerae* population becomes entangled with *E. coli* in well-mixed colonies that fail to develop *V. cholerae*'s normal packing structure, instead growing into disordered, loosely assembled groups that are fully susceptible to predation. This observation clarifies why *V. cholerae* predation protection declines in biofilm co-culture with *E. coli*.

<u>Mixed species cell groups follow distinct trajectories depending on surface colonization conditions</u>

To better understand how the highly packed versus disordered dual-species colonies originate, we ran new experiments tracking biofilm growth at 1 h intervals from the initial stages of surface colonization to the maturation of clusters containing hundreds of cells at 48 h (SI Movie S1). Examples of the two cell group types were found by visual inspection at 48 h and then traced back to their initial condition corresponding to 9h after the start of incubation (Figure 4 A,C; SI Movies S2,S3). On larger spatial scales than shown in Figure 4, both types of colony morphology could be found in close proximity (SI Figure S6). The two colony types could be reliably distinguished by their combined cell packing, which was systematically lower in the core regions of disordered colonies (Figure 4B,D, see below for temporally resolved detail). The two colony structures were also consistently different in total biovolume and species composition, with ordered high-packing cell groups growing to larger population sizes and containing higher relative abundance of *V. cholerae* compared to *E. coli* (Figure 4 E,F).

Though the two biofilm architectures could be quantitatively separated in many respects, the mean distance between *V. cholerae* and *E. coli* cells was the most pronounced factor at early time points that

220 differentiated between cell groups that would become highly packed versus disordered cell groups (Figure 4G; SI Figure S7). The two cell group types in fact begin and remain on different trajectories with respect to *V. cholerae-E. coli* distance across all replicate colony time series acquisitions. *V. cholerae* that produced ordered, highly packed architecture were on average 8 μm away from the nearest *E. coli* cell at early time points, while those that became disordered clusters were only 1 μm from the nearest *E. coli* cell at early
225 time points (Figure 4G,H). This observation suggests that the colonization conditions at the beginning of biofilm growth, as surface-attached cells are just starting to divide in place, are crucial for the eventual consolidation of *V. cholerae* packing architecture.

Reviewing the data obtained from time series of the two dual species colony structures, we also noted an important transition that occurs in ordered high-packing *V. cholerae* cell groups. In our culture
230 conditions at ~19-26 h, a core region of highly packed *V. cholerae* cells is nucleated (Figure 4I), creating a secondary front of structural consolidation that lags behind the outermost growth front in which cell packing is lower (Figure 4B). This secondary front has been observed previously, and it corresponds to the region with sufficiently high cell density to provide predator protection[27,28,78]. In disordered colonies containing well-mixed *V. cholerae* and *E. coli*, the nucleation of this high-density core never occurs. This difference
235 between the two cell group types can be tracked quantitatively via the cell packing of the inner core of each sample (Figure 4J). In ordered colonies, once the highly packed core was initiated, it was stable over time, and interruption of this core nucleation process only occurred if *V. cholerae* and *E. coli* cells happened to begin growing in close proximity from the start of biofilm formation. Allowing *V. cholerae* to grow on its own for 48 h, followed by invasion of *E. coli* into the biofilm environment, never led to any observable
240 disruption of highly packed *V. cholerae* groups. In this scenario, *E. coli* was excluded from pre-formed *V. cholerae* colonies and completely susceptible to predation if *B. bacteriovorus* was later introduced (SI Figure S8).

Our results here highlight critical points for the production of *V. cholerae* biofilm structure with its characteristic packing and cell alignment architecture[27–29,34,78], which in turn are necessary for protection
245 from *B. bacteriovorus*[35]. If *V. cholerae* cells are sufficiently isolated during early biofilm formation, they can grow, divide, and secrete biofilm matrix components that effectively coordinate their normal architecture. However, if *V. cholerae* cells are too close to *E. coli* at the start of biofilm formation, the two species become entangled in the process of growth and division in a manner that interrupts the longer-term production of cell group architecture that *V. cholerae* normally produces on its own. The disruption of the
250 structure that *V. cholerae* typically produces suggests that if *E. coli* is in close enough proximity at early stages of growth, *V. cholerae* either does not upregulate its VPS-dependent biofilm regulon, or the VPS regulon is activated, but with a disruption of the cell-cell orientation and coordination of matrix localization that *V. cholerae* would obtain on its own. The precise genetic and biochemical basis for how biofilm architectural coordination is altered or disrupted outright in multi-species relative to mono-species contexts
255 is an important question for future work.

As highly packed *V. cholerae* cell groups are protected from *B. bacteriovorus*, while disordered colonies are not, our observations lead to the prediction that initial surface colonization conditions, via their impact on the relative proportion of highly packed versus disordered dual species colonies, can dramatically impact the population dynamics of predator-prey interaction.

260

Surface colonization strongly impacts population dynamics via its influence on biofilm architecture

Our results above suggest that the average distance between *V. cholerae* and *E. coli* cells at the start of biofilm growth should directly determine the relative occurrence of highly packed *V. cholerae* groups that incorporate pockets of *E. coli* as they expand, as opposed to disordered dual-species cell groups. In this sense the initial surface coverage should indirectly determine the overall impact of predation on survival of both species via its direct impact on colony structure development. We tested this prediction by inoculating two sets of two-species chambers with relatively low or high surface colonization density (20% versus 60% surface coverage, respectively, SI Figure S9A). Low or high initial density alters the average distance between *V. cholerae* and *E. coli* cells (SI Figure S9B), in turn leading to large volumes of highly packed *V. cholerae* colonies containing small numbers of *E. coli* (low initial density), or almost exclusively disordered, mixed colonies containing homogeneously distributed *V. cholerae* and *E. coli* (Figure 5A,B). As anticipated, low versus high initial surface occupation led to different population dynamical outcomes after the introduction of *B. bacteriovorus*. In the low initial density condition, the majority of *V. cholerae*, as well as the smaller groups of *E. coli* embedded in their packed biofilms, survive predator exposure (Figure 5C,E,F). By contrast, in the high initial density conditions predominated by disordered groups of *V. cholerae* and *E. coli*, almost the entire dual species prey community is killed off following the introduction *B. bacteriovorus* (Figure 5D-F). Taken together, these data strongly support our prediction that surface colonization conditions determine the relative fractions of ordered versus disordered biofilm cell groups of *E. coli* and *V. cholerae*, which in turn governs the survival of both prey species under *B. bacteriovorus* predation.

Discussion

Exploration of multi-species biofilm communities using live high-resolution imaging is crucial to understanding microbial ecology at the spatial scale on which cell-cell interactions occur [11,20,23,79–88]. Here we tracked the spatial population dynamics of the bacterial predator *B. bacteriovorus* in dual-species prey biofilms of *V. cholerae* and *E. coli*, finding that the survival rates of both prey species are substantially altered, but in opposite directions, when they are growing together. *V. cholerae* produces biofilm cell clusters that reach a cell packing density threshold past which *B. bacteriovorus* cannot enter, protecting the prey within. *E. coli* can become enveloped within these highly packed structures, co-opting predator protection from *V. cholerae* and increasing *E. coli* survival relative to when growing on its own. By contrast, in dual species biofilms, a fraction of *V. cholerae* becomes entangled with *E. coli* early during biofilm growth, leading to an alternate structure that is homogeneously mixed, disordered, and loosely packed. These disordered cell groups do not block predator cell entry, and all prey within them are killed by *B. bacteriovorus*. As a result of these biofilm structural dynamics, *V. cholerae* survival decreases in co-culture with *E. coli* relative to when growing on its own. At any given location, which of these two alternative cell group structures emerges depends on the initial distance between *V. cholerae* and *E. coli* cells that have attached to the underlying surface. Surface colonization density therefore determines the relative occurrence of predation-protected cell groups versus susceptible cell groups, and the overall rates of *B. bacteriovorus* predator survival for each prey species.

This study makes explicit that the cellular arrangement and tightly packed structure of clonal *V. cholerae* groups can operate as a type of public good that confers predator protection to the cells within

(among many benefits [30,30,33–35,55,74,89–93]). Other species – here, *E. coli*, whose mono-species biofilms are susceptible to *B. bacteriovorus* – can take advantage of this protective architecture when small groups of them become enveloped by expanding, highly packed biofilms of *V. cholerae*. By contrast, if too many *E. coli* cells are present in close enough proximity to *V. cholerae* at the start of biofilm growth, then *V. cholerae* cannot initiate its normal cell group structure, and the public good benefit of predation protection completely breaks down in that location. It is notable that the spatial architecture of biofilm-producing bacteria can manifest as a public good that is exploitable across species in this manner. In this case the stability of *V. cholerae* cooperative architecture depends on the initial surface population density, which determines whether *V. cholerae* cell lineages have enough space to nucleate the highly packed core regions of expanding biofilm clusters before encountering cells of other species. Though distinct in mechanistic detail, this example should fall under related social evolution principles as other kinds of microbial cooperation that provide benefits in a distance-dependent manner. Recent work has highlighted in detail how the population dynamics and evolutionary stability of this class of cooperative behavior depends on the spatial range of cooperative sharing, the population/community composition, and spatial cell arrangements during early biofilm growth[33,34,89,92,94,95] .

The interplay of *V. cholerae*, *E. coli*, and *B. bacteriovorus* in co-culture emphasizes that the population dynamics of different species in a community can depend quite strongly on the cellular resolution details of biofilm structure, which in turn can differ in unexpected ways between mono-species and multi-species systems. In recent years microbiologists have made tremendous strides in understanding the cellular and molecular nuances of biofilm architecture and their relationship to microbial ecology and evolution. By necessity for tractability in many cases, much of this work has focused on one species at a time. Our experiments here highlight how new and interesting questions about the drivers of biofilm structure, and the relationship between biofilm structure and community ecology, can arise from modest increases in complexity with multi-species systems. Here, it appears as though *E. coli* – if adjacent to *V. cholerae* at the start of biofilm growth – likely interferes with normal localization of *V. cholerae* matrix localization and cell-cell alignment that are critical at early stages of biofilm growth for establishing their normal architecture. The connection between initial surface coverage and multispecies prey biofilm architecture, and the connection between architecture and predator exposure, leads to an interesting dependence between early biofilm growth conditions and predator-prey ecology that would be fruitful to explore further in other systems.

Where prior studies have analyzed multispecies biofilms at high resolution, they have also indicated important consequences for community structure and environmental impacts[11,12,22,47,48,96–100] . A notable recent example examined the detailed structure of multispecies biofilm communities growing as plaque associated with dental caries[48] . Kim et al. showed that *Streptococcus mutans* forms consistent spatial arrangements in biofilm co-culture with other oral microbiota species. In this case, *S. mutans* consistently produce core clonal regions, around which form layers of non-*mutans* streptococci followed by non-streptococci. The metabolic activity of *S. mutans* within the inner regions of these multispecies biofilms caused low local pH that could recapitulate the rapid demineralization of enamel that occurs during development of caries.

Collective behavior can involve multiple species interacting in groups across the biological world, including among animals moving on much larger spatial scales that we observe here[101–103] . Though bacteria

and metazoans are obviously quite different in their scale, movement, and behavior, some common principles do emerge. In mixed species herds, for example, prey animals may gain heightened protection from predators within groups of another species with superior predator detection abilities in order to benefit from earlier warnings of approaching threats[104] . In some cases the presence of the secondary species, as it does here when *E. coli* is intertwined with *V. cholerae* in disordered cell groups, may increase local competition for space and interfere with the primary species' predator avoidance mechanism. We envision that this is just one of many new connections between collective behavior across scales that may emerge from further study of predation in microbial multispecies prey environments.

Acknowledgements

We are grateful to James Winans, Blair Costelloe, Robert Cramer, Matthew Ayres, and Jing Yan for helpful advice on earlier versions of the manuscript, and to members of the Nadell Lab at Dartmouth for their input during development of the experiments and analysis. BRW is supported by a Gillman Fellowship from the Department of Biological Sciences at Dartmouth. CDN is supported by the Simons Foundation award number 826672, NSF grant IOS 2017879, NSF grant MCB 1817352, and grant RGY0077/2020 from the Human Frontier Science Program.

Author Contributions

BRW and CDN conceived the study and designed experiments. CDN acquired funding for the work and supervised the project. ME and DEK provided new reagents/tools. BRW performed experiments and image processing of microscopy data. BRW and CDN analyzed data, produced the figures, and wrote the paper.

Materials and Methods

Microfluidic assembly

Microfluidic chambers for biofilm growth were produced with polydimethylsiloxane (PDMS) using standard soft lithography techniques[105,106]. PDMS was cured on molds of chamber sets, which were then cut out and bonded to a #1.5 36mm by 60mm glass coverslip using plasma cleaning treatment of the bonding sides of the PDMS chambers and coverslip glass. Biofilm growth chambers in this study measured 3000µm x 500µm x 75µm (LxWxD). Flow was manipulated using Harvard Apparatus Pico Plus syringe pumps loaded with 1ml BD plastic syringes. These syringes had 25-gauge needles affixed to them that were fitted with #30 Cole Palmer PTFE tubing with an inner diameter of 0.3mm. Tubing lines were placed into the inlet of each biofilm growth chamber, with outlet tubing feeding to liquid waste containers.

Bacterial culture conditions

V. cholerae N16961 and *E. coli* AR3110 were all grown overnight in lysogeny broth (LB) in shaking culture conditions at 37ºC. *B. bacteriovorus* 109J stocks were obtained via co-culture with prey and filtering as described previously[35].

Biofilm growth and matrix immunofluorescence

To introduce bacteria to the microfluidic device, overnight cultures of *V. cholerae* and *E. coli* were diluted and regrown in fresh media to a OD_{600} = 1.0 and inoculated into the chamber via micropipette. The

inoculating cultures were left to stand in the chambers for 1h without flow to allow for surface colonization. Flow of M9 minimal media with 0.5% glucose was then initiated at 0.2μL/min. For dual species prey biofilms with *V. cholerae* and *E. coli* inoculated together, cultures of each species were each diluted to OD_{600} = 1.0 and mixed 1:1 just prior to inoculation into chambers.

Bacterial predator introduction and invading bacterial introduction

To introduce bacterial predators, *B bacteriovorus* were equalized to an OD_{600} = 1.0 (2.5 x 10^9 PFU/mL) using M9 with 0.5% glucose. These cultures were then loaded into 1ml syringes. At the time of predator inoculation, the syringe and tubing containing sterile media were changed for the syringe and tubing containing predators, and flow was resumed at 0.2μL/min. After 1h, the tubing was changed back to an influx of sterile M9 with 0.5% glucose. For the introduction of invading *E. coli* (SI Figure S8), cultures of *E. coli* were concentrated to an OD_{600} = 5.0 prior to inoculation and loaded into 1ml syringes. A similar tubing swap was performed as described above and *E. coli* flow was allowed to continue for 24h. After 24h, the syringe and tubing were replaced with media containing predators as described above. After 1h of predator introduction, the syringe and tubing containing sterile M9 media with 0.5% glucose were replaced once again to resume sterile medium influx.

Bacterial dispersal and re-colonization

To disperse biofilms and test for downstream re-colonization, the flow rate of the microfluidic devices was increased from 0.2 μl/min to 100 μl/min (mean flow velocity increased from 90 μm/s to 45,000 μm/s). Effluent from this period was connected to a new, sterile microfluidic device, and high flow was allowed to continue for 5 min. After this period, sterile M9 minimal media with 0.5% glucose was introduced to the new device at a flow rate of 0.2 μL/min.

Microscopy and image analysis

Imaging was performed on Zeiss LSM 880 and LSM 980 laser scanning confocal microscopes. Both instruments were fitted with a 40x/ 1.2 N.A. water objective and a 10x/ 0.4 N.A. water objective. 488nm, 543nm, and 594nm laser lines were used to excite the fluorescent proteins mGFP, mKO-k, and mKate2, respectively. The hardware was controlled by ZEN Black for the 880 and ZEN blue for the 980. To obtain data for image analysis, several image stacks were taken across biological replicates in independent chambers. Prior to export, the channels were processed by linear unmixing and constrained iterative deconvolution (Poisson likelihood, Zero order regularization, Newton Raphson optimization, maximum 40 iteration, 0.1% quality threshold, scalar theory PSF generation) in ZEN blue. These images were then exported and analyzed using BiofilmQ. 3d image renderings were produced using Zen or VTK export from BiofilmQ and subsequent processing in ParaView.

Quantification and statistics

Biofilms were segmented using the image analysis framework BiofilmQ[107]. Briefly, BiofilmQ denoises image data and segments biovolume into pseudo-cell cubes that can be used for image spatially resolved

425 data analysis. Files were imported Directly from ZEN. For population level experiments, total biovolume of each species was tracked. For data involving micro-scale architecture, only 40x data were used and were segmented into cubes with a volume of 2.06μm^3. Cell packing was determined using a local density calculation with a spatial range of 6μm. This is the spatial scale – neighborhood volume fraction – that we have previously shown to be most relevant pertinent to measuring packing-based protection against *B.*
430 *bacteriovorus*. Degree of predation was obtained by calculating Mander's overlap coefficients between the prey species and *B. bacteriovorus*. If any amount of predator signal is detected within prey signal, the degree of predation will be above 0. For pairwise comparisons, Mann-Whitney U-tests with Bonferroni correction were performed. For frequency distribution comparisons, we used Kolmogorov-Smirnov tests.

435

Reagent or Resource	**Source**	**Identifier**
Antibodies		
Cy3 conjugated anti-FLAG	Millipore-Sigma	Cat#A9594
Bacterial Strains and Viruses		
E coli AR 3110, *lacZ*:Ptac-mKO-κ		Strain CNE 689
B. bacteriovorus 109J, PMQ581, gfpmut3	This study	Strain 109J
V. cholerae N16961 *rbmA*-3xFLAG, *lacZ*:Ptac-mKate2	[108]	Strain CNV 116
V. cholerae N16961 *rbmC*-3xFLAG, *lacZ*:Ptac-mKate2	[108]	Strain CNV 117
V. cholerae N16961 *bap1*-3xFLAG, *lacZ*:Ptac-mKate2	[108]	Strain CNV 119
V. cholerae N16961 *rbmA*-3xFLAG, *lacZ*:Ptac-mKO-κ	[108]	Strain CNV 121
V. cholerae N16961, *lacZ*:Ptac-mKate2 *ΔrbmA*	[108]	Strain CNV 127
Chemicals, Peptides and Recombinant Proteins		
Ampicillin	Millipore-Sigma	Cat#A0166
Kanamycin	Millipore-Sigma	Cat#60615
Polymyxin B	Millipore-Sigma	Cat#P4932
MEM Vitamins Solution (100x)	Millipore-Sigma	Cat#M6895
Recombinant DNA		
pMQ581 Constructed by replacement of *tdTomato* with *gfpmut3* in pMQ414 parental plasmid	[109]	Plasmid pMQ581
Software and Algorithms		
ZEN Black	Zeiss	Version 2.3
ZEN Blue	Zeiss	Version 2.3
MATLAB	MathWorks	Version R2018b
Paraview	Kitware	Version 5.1.2
Prism	GraphPad	Version 7.02
BiofilmQ	[110]	Version 0.2.2
R	glm, 'car' package	Version 4.0.2

References

(1) Mayr, E. 80 Years of Watching the Evolutionary Scenery. *Science* **2004**, *305* (5680), 46–47. https://doi.org/10.1126/science.1100561.

(2) Cordero, O. X.; Datta, M. S. Microbial Interactions and Community Assembly at Microscales. *Curr. Opin. Microbiol.* **2016**, *31*, 227–234. https://doi.org/10.1016/j.mib.2016.03.015.

(3) Gralka, M.; Szabo, R.; Stocker, R.; Cordero, O. X. Trophic Interactions and the Drivers of Microbial Community Assembly. *Curr. Biol. CB* **2020**, *30* (19), R1176–R1188. https://doi.org/10.1016/j.cub.2020.08.007.

(4) Hibbing, M. E.; Fuqua, C.; Parsek, M. R.; Peterson, S. B. Bacterial Competition: Surviving and Thriving in the Microbial Jungle. *Nat. Rev. Microbiol.* **2010**, *8* (1), 15–25. https://doi.org/10.1038/nrmicro2259.

(5) Datta, M. S.; Sliwerska, E.; Gore, J.; Polz, M. F.; Cordero, O. X. Microbial Interactions Lead to Rapid Micro-Scale Successions on Model Marine Particles. *Nat. Commun.* **2016**, *7* (1), 11965–11965. https://doi.org/10.1038/ncomms11965.

(6) Yawata, Y.; Cordero, O. X.; Menolascina, F.; Hehemann, J.-H.; Polz, M. F.; Stocker, R. Competition-Dispersal Tradeoff Ecologically Differentiates Recently Speciated Marine Bacterioplankton Populations. *Proc. Natl. Acad. Sci.* **2014**, *111* (15), 5622–5627. https://doi.org/10.1073/pnas.1318943111.

(7) Shu, W.-S.; Huang, L.-N. Microbial Diversity in Extreme Environments. *Nat. Rev. Microbiol.* **2022**, *20* (4), 219–235. https://doi.org/10.1038/s41579-021-00648-y.

(8) de Dios Caballero, J.; Vida, R.; Cobo, M.; Máiz, L.; Suárez, L.; Galeano, J.; Baquero, F.; Cantón, R.; Del Campo, R. Individual Patterns of Complexity in Cystic Fibrosis Lung Microbiota, Including Predator Bacteria, over a 1-Year Period. *mBio* **2017**, *8* (5). https://doi.org/10.1128/mBio.00959-17.

(9) Alavi, S.; Mitchell, J. D.; Cho, J. Y.; Liu, R.; Macbeth, J. C.; Hsiao, A. Interpersonal Gut Microbiome Variation Drives Susceptibility and Resistance to Cholera Infection. *Cell* **2020**, *181* (7), 1533-1546.e13. https://doi.org/10.1016/j.cell.2020.05.036.

(10) Wolff, R.; Shoemaker, W.; Garud, N. *Ecological Stability Emerges at the Level of Strains in the Human Gut Microbiome*; 2021; p 2021.09.30.462616. https://doi.org/10.1101/2021.09.30.462616.

(11) Earle, K. A.; Billings, G.; Sigal, M.; Lichtman, J. S.; Hansson, G. C.; Elias, J. E.; Amieva, M. R.; Huang, K. C.; Sonnenburg, J. L. Quantitative Imaging of Gut Microbiota Spatial Organization. *Cell Host Microbe* **2015**, *18* (4), 478–488. https://doi.org/10.1016/j.chom.2015.09.002.

(12) Mark Welch, J. L.; Hasegawa, Y.; McNulty, N. P.; Gordon, J. I.; Borisy, G. G. Spatial Organization of a Model 15-Member Human Gut Microbiota Established in Gnotobiotic Mice. *Proc. Natl. Acad. Sci.* **2017**, *114* (43), E9105–E9114. https://doi.org/10.1073/pnas.1711596114.

(13) Jakubovics, N. S.; Goodman, S. D.; Mashburn-Warren, L.; Stafford, G. P.; Cieplik, F. The Dental Plaque Biofilm Matrix. *Periodontol. 2000* **2021**, *86* (1), 32–56. https://doi.org/10.1111/prd.12361.

(14) Marsh, P. D. Dental Plaque as a Biofilm and a Microbial Community – Implications for Health and Disease. *BMC Oral Health* **2006**, *6* (1), S14. https://doi.org/10.1186/1472-6831-6-S1-S14.

(15) Frost, L. R.; Cheng, J. K. J.; Unnikrishnan, M. Clostridioides Difficile Biofilms: A Mechanism of Persistence in the Gut? *PLOS Pathog.* **2021**, *17* (3), e1009348. https://doi.org/10.1371/journal.ppat.1009348.

(16) Béchon, N.; Ghigo, J.-M. Gut Biofilms: Bacteroides as Model Symbionts to Study Biofilm Formation by Intestinal Anaerobes. *FEMS Microbiol. Rev.* **2022**, *46* (2), fuab054. https://doi.org/10.1093/femsre/fuab054.

(17) Flemming, H.-C. Biofouling in Water Systems – Cases, Causes and Countermeasures. *Appl. Microbiol. Biotechnol.* **2002**, *59* (6), 629–640. https://doi.org/10.1007/s00253-002-1066-9.

(18) Huang, H.; Peng, C.; Peng, P.; Lin, Y.; Zhang, X.; Ren, H. Towards the Biofilm Characterization and Regulation in Biological Wastewater Treatment. *Appl. Microbiol. Biotechnol.* **2019**, *103* (3), 1115–1129. https://doi.org/10.1007/s00253-018-9511-6.

(19) Boltz, J. P.; Smets, B. F.; Rittmann, B. E.; van Loosdrecht, M. C. M.; Morgenroth, E.; Daigger, G. T. From Biofilm Ecology to Reactors: A Focused Review. *Water Sci. Technol. J. Int. Assoc. Water Pollut. Res.* **2017**, *75* (7–8), 1753–1760. https://doi.org/10.2166/wst.2017.061.

(20) Burmølle, M.; Hansen, L. H.; Sørensen, S. J. Establishment and Early Succession of a Multispecies Biofilm Composed of Soil Bacteria. *Microb. Ecol.* **2007**, *54* (2), 352–362. https://doi.org/10.1007/s00248-007-9222-5.

(21) Dang, H.; Lovell, C. R. Microbial Surface Colonization and Biofilm Development in Marine Environments. *Microbiol. Mol. Biol. Rev. MMBR* **2016**, *80* (1), 91–138. https://doi.org/10.1128/MMBR.00037-15.

(22) Leventhal, G. E.; Boix, C.; Kuechler, U.; Enke, T. N.; Sliwerska, E.; Holliger, C.; Cordero, O. X. Strain-Level Diversity Drives Alternative Community Types in Millimetre-Scale Granular Biofilms. *Nat. Microbiol.* **2018**, *3* (11), 1295–1303. https://doi.org/10.1038/s41564-018-0242-3.
(23) Mitri, S.; Xavier, J. B.; Foster, K. R. Social Evolution in Multispecies Biofilms. *Proc. Natl. Acad. Sci.* **2011**, *108* (supplement_2), 10839–10846. https://doi.org/10.1073/pnas.1100292108.
(24) Rao, D.; Webb, J. S.; Kjelleberg, S. Competitive Interactions in Mixed-Species Biofilms Containing the Marine Bacterium Pseudoalteromonas Tunicata. *Appl. Environ. Microbiol.* **2005**, *71* (4), 1729–1736. https://doi.org/10.1128/AEM.71.4.1729-1736.2005.
(25) Wucher, B. R.; Bartlett, T. M.; Hoyos, M.; Papenfort, K.; Persat, A.; Nadell, C. D. Vibrio Cholerae Filamentation Promotes Chitin Surface Attachment at the Expense of Competition in Biofilms. *Proc. Natl. Acad. Sci.* **2019**, *116* (28), 14216–14221. https://doi.org/10.1073/pnas.1819016116.
(26) Absalon, C.; Van Dellen, K.; Watnick, P. I. A Communal Bacterial Adhesin Anchors Biofilm and Bystander Cells to Surfaces. *PLoS Pathog.* **2011**, *7* (8), e1002210–e1002210. https://doi.org/10.1371/journal.ppat.1002210.
(27) Berk, V.; Fong, J. C. N.; Dempsey, G. T.; Develioglu, O. N.; Zhuang, X.; Liphardt, J.; Yildiz, F. H.; Chu, S. Molecular Architecture and Assembly Principles of Vibrio Cholerae Biofilms. *Science* **2012**, *337* (6091), 236–239. https://doi.org/10.1126/science.1222981.
(28) Drescher, K.; Dunkel, J.; Nadell, C. D.; van Teeffelen, S.; Grnja, I.; Wingreen, N. S.; Stone, H. A.; Bassler, B. L. Architectural Transitions in Vibrio Cholerae Biofilms at Single-Cell Resolution. *Proc. Natl. Acad. Sci.* **2016**, *113* (14), E2066–E2072. https://doi.org/10.1073/pnas.1601702113.
(29) Yan, J.; Sharo, A. G.; Stone, H. A.; Wingreen, N. S.; Bassler, B. L. Vibrio Cholerae Biofilm Growth Program and Architecture Revealed by Single-Cell Live Imaging. *Proc. Natl. Acad. Sci.* **2016**, *113* (36), E5337–E5343. https://doi.org/10.1073/pnas.1611494113.
(30) Tai, J.-S. B.; Mukherjee, S.; Nero, T.; Olson, R.; Tithof, J.; Nadell, C. D.; Yan, J. Social Evolution of Shared Biofilm Matrix Components. *Proc. Natl. Acad. Sci.* **2022**, *119* (27), e2123469119. https://doi.org/10.1073/pnas.2123469119.
(31) Ma, L.; Conover, M.; Lu, H.; Parsek, M. R.; Bayles, K.; Wozniak, D. J. Assembly and Development of the Pseudomonas Aeruginosa Biofilm Matrix. *PLOS Pathog.* **2009**, *5* (3), e1000354. https://doi.org/10.1371/journal.ppat.1000354.
(32) Reichhardt, C.; Parsek, M. R. Confocal Laser Scanning Microscopy for Analysis of Pseudomonas Aeruginosa Biofilm Architecture and Matrix Localization. *Front. Microbiol.* **2019**, *10*.
(33) Drescher, K.; Nadell, C. D.; Stone, H. A.; Wingreen, N. S.; Bassler, B. L. Solutions to the Public Goods Dilemma in Bacterial Biofilms. *Curr. Biol.* **2014**, *24* (1), 50–55. https://doi.org/10.1016/j.cub.2013.10.030.
(34) Nadell, C. D.; Drescher, K.; Wingreen, N. S.; Bassler, B. L. Extracellular Matrix Structure Governs Invasion Resistance in Bacterial Biofilms. *ISME J.* **2015**, *9* (8), 1700–1709. https://doi.org/10.1038/ismej.2014.246.
(35) Wucher, B. R.; Elsayed, M.; Adelman, J. S.; Kadouri, D. E.; Nadell, C. D. Bacterial Predation Transforms the Landscape and Community Assembly of Biofilms. *Curr. Biol. CB* **2021**, *31* (12), 2643-2651.e3. https://doi.org/10.1016/j.cub.2021.03.036.
(36) Kadouri, D.; O'Toole, G. A. Susceptibility of Biofilms to Bdellovibrio Bacteriovorus Attack. *Appl. Environ. Microbiol.* **2005**, *71* (7), 4044–4051. https://doi.org/10.1128/AEM.71.7.4044-4051.2005.
(37) Díaz-Pascual, F.; Hartmann, R.; Lempp, M.; Vidakovic, L.; Song, B.; Jeckel, H.; Thormann, K. M.; Yildiz, F. H.; Dunkel, J.; Link, H.; Nadell, C. D.; Drescher, K. Breakdown of Vibrio Cholerae Biofilm Architecture Induced by Antibiotics Disrupts Community Barrier Function. *Nat. Microbiol.* **2019**, *4* (12), 2136–2145. https://doi.org/10.1038/s41564-019-0579-2.
(38) Nadell, C. D.; Bassler, B. L. A Fitness Trade-off between Local Competition and Dispersal in Vibrio Cholerae Biofilms. *Proc. Natl. Acad. Sci.* **2011**, *108* (34), 14181–14185. https://doi.org/10.1073/pnas.1111147108.
(39) Nadell, C. D.; Drescher, K.; Foster, K. R. Spatial Structure, Cooperation and Competition in Biofilms. *Nat. Rev. Microbiol.* **2016**, *14* (9), 589–600. https://doi.org/10.1038/nrmicro.2016.84.
(40) Giglio, K. M.; Fong, J. C.; Yildiz, F. H.; Sondermann, H. Structural Basis for Biofilm Formation via the Vibrio Cholerae Matrix Protein RbmA. *J. Bacteriol.* **2013**, *195* (14), 3277–3286. https://doi.org/10.1128/JB.00374-13.

(41) Nadell, C. D.; Xavier, J. B.; Foster, K. R. The Sociobiology of Biofilms. *FEMS Microbiol. Rev.* **2009**, *33* (1), 206–224. https://doi.org/10.1111/j.1574-6976.2008.00150.x.
(42) Arnaouteli, S.; Bamford, N. C.; Stanley-Wall, N. R.; Kovács, Á. T. Bacillus Subtilis Biofilm Formation and Social Interactions. *Nat. Rev. Microbiol.* **2021**, *19* (9), 600–614. https://doi.org/10.1038/s41579-021-00540-9.
(43) Abee, T.; Kovács, Á. T.; Kuipers, O. P.; van der Veen, S. Biofilm Formation and Dispersal in Gram-Positive Bacteria. *Curr. Opin. Biotechnol.* **2011**, *22* (2), 172–179. https://doi.org/10.1016/j.copbio.2010.10.016.
(44) Maier, B.; Wong, G. C. L. How Bacteria Use Type IV Pili Machinery on Surfaces. *Trends Microbiol.* **2015**, *23* (12), 775–788. https://doi.org/10.1016/j.tim.2015.09.002.
(45) Oldewurtel, E. R.; Kouzel, N.; Dewenter, L.; Henseler, K.; Maier, B. Differential Interaction Forces Govern Bacterial Sorting in Early Biofilms. *eLife* **2015**, *4*, e10811. https://doi.org/10.7554/eLife.10811.
(46) Reichhardt, C.; Wong, C.; Passos da Silva, D.; Wozniak, D. J.; Parsek, M. R. CdrA Interactions within the Pseudomonas Aeruginosa Biofilm Matrix Safeguard It from Proteolysis and Promote Cellular Packing. *mBio* **2018**, *9* (5), e01376-18. https://doi.org/10.1128/mBio.01376-18.
(47) Mark Welch, J. L.; Rossetti, B. J.; Rieken, C. W.; Dewhirst, F. E.; Borisy, G. G. Biogeography of a Human Oral Microbiome at the Micron Scale. *Proc. Natl. Acad. Sci.* **2016**, *113* (6), E791–E800. https://doi.org/10.1073/pnas.1522149113.
(48) Kim, D.; Barraza, J. P.; Arthur, R. A.; Hara, A.; Lewis, K.; Liu, Y.; Scisci, E. L.; Hajishengallis, E.; Whiteley, M.; Koo, H. Spatial Mapping of Polymicrobial Communities Reveals a Precise Biogeography Associated with Human Dental Caries. *Proc. Natl. Acad. Sci.* **2020**, *117* (22), 12375–12386. https://doi.org/10.1073/pnas.1919099117.
(49) Mondragón-Palomino, O.; Poceviciute, R.; Lignell, A.; Griffiths, J. A.; Takko, H.; Ismagilov, R. F. Three-Dimensional Imaging for the Quantification of Spatial Patterns in Microbiota of the Intestinal Mucosa. *Proc. Natl. Acad. Sci. U. S. A.* **2022**, *119* (18), e2118483119. https://doi.org/10.1073/pnas.2118483119.
(50) Lopez, J. G.; Wingreen, N. S. Noisy Metabolism Can Promote Microbial Cross-Feeding. *eLife* **2022**, *11*, e70694. https://doi.org/10.7554/eLife.70694.
(51) Díaz-Pascual, F.; Lempp, M.; Nosho, K.; Jeckel, H.; Jo, J. K.; Neuhaus, K.; Hartmann, R.; Jelli, E.; Hansen, M. F.; Price-Whelan, A.; Dietrich, L. E.; Link, H.; Drescher, K. Spatial Alanine Metabolism Determines Local Growth Dynamics of Escherichia Coli Colonies. *eLife* **2021**, *10*, e70794. https://doi.org/10.7554/eLife.70794.
(52) Drebes Dörr, N. C.; Blokesch, M. Bacterial Type VI Secretion System Facilitates Niche Domination. *Proc. Natl. Acad. Sci.* **2018**, *115* (36), 8855–8857. https://doi.org/10.1073/pnas.1812776115.
(53) Smith, W. P. J.; Brodmann, M.; Unterweger, D.; Davit, Y.; Comstock, L. E.; Basler, M.; Foster, K. R. The Evolution of Tit-for-Tat in Bacteria via the Type VI Secretion System. *Nat. Commun.* **2020**, *11* (1), 5395. https://doi.org/10.1038/s41467-020-19017-z.
(54) Granato, E. T.; Meiller-Legrand, T. A.; Foster, K. R. The Evolution and Ecology of Bacterial Warfare. *Curr. Biol. CB* **2019**, *29* (11), R521–R537. https://doi.org/10.1016/j.cub.2019.04.024.
(55) Tseng, B. S.; Zhang, W.; Harrison, J. J.; Quach, T. P.; Song, J. L.; Penterman, J.; Singh, P. K.; Chopp, D. L.; Packman, A. I.; Parsek, M. R. The Extracellular Matrix Protects Pseudomonas Aeruginosa Biofilms by Limiting the Penetration of Tobramycin. *Environ. Microbiol.* **2013**, *15* (10), 2865–2878. https://doi.org/10.1111/1462-2920.12155.
(56) Wang, Y.; Cheng, L. I.; Helfer, D. R.; Ashbaugh, A. G.; Miller, R. J.; Tzomides, A. J.; Thompson, J. M.; Ortines, R. V.; Tsai, A. S.; Liu, H.; Dillen, C. A.; Archer, N. K.; Cohen, T. S.; Tkaczyk, C.; Stover, C. K.; Sellman, B. R.; Miller, L. S. Mouse Model of Hematogenous Implant-Related Staphylococcus Aureus Biofilm Infection Reveals Therapeutic Targets. *Proc. Natl. Acad. Sci. U. S. A.* **2017**, *114* (26), E5094–E5102. https://doi.org/10.1073/pnas.1703427114.
(57) Dashiff, A.; Junka, R. A.; Libera, M.; Kadouri, D. E. Predation of Human Pathogens by the Predatory Bacteria Micavibrio Aeruginosavorus and Bdellovibrio Bacteriovorus. *J. Appl. Microbiol.* **2011**, *110* (2), 431–444. https://doi.org/10.1111/j.1365-2672.2010.04900.x.
(58) Otto, S.; Bruni, E. P.; Harms, H.; Wick, L. Y. Catch Me If You Can: Dispersal and Foraging of Bdellovibrio Bacteriovorus 109J along Mycelia. *ISME J.* **2017**, *11* (2), 386–393. https://doi.org/10.1038/ismej.2016.135.
(59) Sockett, R. E. Predatory Lifestyle of Bdellovibrio Bacteriovorus. *Annu. Rev. Microbiol.* **2009**, *63*, 523–539. https://doi.org/10.1146/annurev.micro.091208.073346.

(60) Summers, J. K.; Kreft, J.-U. Predation Strategies of the Bacterium Bdellovibrio Bacteriovorus Result in Bottlenecks, Overexploitation, Minimal and Optimal Prey Sizes. *bioRxiv* **2019**, 621490. https://doi.org/10.1101/621490.
(61) Evans, K. J.; Lambert, C.; Sockett, R. E. Predation by Bdellovibrio Bacteriovorus HD100 Requires Type IV Pili. *J. Bacteriol.* **2007**, *189* (13), 4850–4859. https://doi.org/10.1128/JB.01942-06.
(62) Duncan, M. C.; Gillette, R. K.; Maglasang, M. A.; Corn, E. A.; Tai, A. K.; Lazinski, D. W.; Shanks, R. M. Q.; Kadouri, D. E.; Camilli, A. High-Throughput Analysis of Gene Function in the Bacterial Predator Bdellovibrio Bacteriovorus. *mBio* **2019**, *10* (3). https://doi.org/10.1128/mBio.01040-19.
(63) Iebba, V.; Totino, V.; Santangelo, F.; Gagliardi, A.; Ciotoli, L.; Virga, A.; Ambrosi, C.; Pompili, M.; De Biase, R. V.; Selan, L.; Artini, M.; Pantanella, F.; Mura, F.; Passariello, C.; Nicoletti, M.; Nencioni, L.; Trancassini, M.; Quattrucci, S.; Schippa, S. Bdellovibrio Bacteriovorus Directly Attacks Pseudomonas Aeruginosa and Staphylococcus Aureus Cystic Fibrosis Isolates. *Front. Microbiol.* **2014**, *5*. https://doi.org/10.3389/fmicb.2014.00280.
(64) Gorelik, O.; Levy, N.; Shaulov, L.; Yegodayev, K.; Meijler, M. M.; Sal-Man, N. Vibrio Cholerae Autoinducer-1 Enhances the Virulence of Enteropathogenic Escherichia Coli. *Sci. Rep.* **2019**, *9* (1), 4122. https://doi.org/10.1038/s41598-019-40859-1.
(65) Abriat, C.; Enriquez, K.; Virgilio, N.; Cegelski, L.; Fuller, G. G.; Daigle, F.; Heuzey, M.-C. Mechanical and Microstructural Insights of Vibrio Cholerae and Escherichia Coli Dual-Species Biofilm at the Air-Liquid Interface. *Colloids Surf. B Biointerfaces* **2020**, *188*, 110786. https://doi.org/10.1016/j.colsurfb.2020.110786.
(66) Chakraborty, S.; Deokule, J. S.; Garg, P.; Bhattacharya, S. K.; Nandy, R. K.; Nair, G. B.; Yamasaki, S.; Takeda, Y.; Ramamurthy, T. Concomitant Infection of Enterotoxigenic Escherichia Coli in an Outbreak of Cholera Caused by Vibrio Cholerae O1 and O139 in Ahmedabad, India. *J. Clin. Microbiol.* **2001**, *39* (9), 3241–3246. https://doi.org/10.1128/JCM.39.9.3241-3246.2001.
(67) Hood, M. A.; Ness, G. E. Survival of Vibrio Cholerae and Escherichia Coli in Estuarine Waters and Sediments. *Appl. Environ. Microbiol.* **1982**, *43* (3), 578–584. https://doi.org/10.1128/aem.43.3.578-584.1982.
(68) Wang, H.; Li, F.; Xu, L.; Byun, H.; Fan, J.; Wang, M.; Li, M.; Zhu, J.; Li, B. Contributions of Escherichia Coli and Its Motility to the Formation of Dual-Species Biofilms with Vibrio Cholerae. *Appl. Environ. Microbiol. 87* (18), e00938-21. https://doi.org/10.1128/AEM.00938-21.
(69) Shikuma, N. J.; Hadfield, M. G. Marine Biofilms on Submerged Surfaces Are a Reservoir for Escherichia Coli and Vibrio Cholerae. *Biofouling* **2010**, *26* (1), 39–46. https://doi.org/10.1080/08927010903282814.
(70) Yildiz, F. H.; Visick, K. L. Vibrio Biofilms: So Much the Same yet so Different. *Trends Microbiol.* **2009**, *17* (3), 109–118. https://doi.org/10.1016/j.tim.2008.12.004.
(71) Teschler, J. K.; Nadell, C. D.; Drescher, K.; Yildiz, F. H. Mechanisms Underlying Vibrio Cholerae Biofilm Formation and Dispersion. *Annu. Rev. Microbiol.* **2022**, *76* (1), null. https://doi.org/10.1146/annurev-micro-111021-053553.
(72) Teschler, J. K.; Zamorano-Sánchez, D.; Utada, A. S.; Warner, C. J. A.; Wong, G. C. L.; Linington, R. G.; Yildiz, F. H. Living in the Matrix: Assembly and Control of Vibrio Cholerae Biofilms. *Nat. Rev. Microbiol.* **2015**, *13* (5), 255–268. https://doi.org/10.1038/nrmicro3433.
(73) Serra, D. O.; Hengge, R. Bacterial Multicellularity: The Biology of Escherichia Coli Building Large-Scale Biofilm Communities. *Annu. Rev. Microbiol.* **2021**, *75* (1), 269–290. https://doi.org/10.1146/annurev-micro-031921-055801.
(74) Vidakovic, L.; Singh, P. K.; Hartmann, R.; Nadell, C. D.; Drescher, K. Dynamic Biofilm Architecture Confers Individual and Collective Mechanisms of Viral Protection. *Nat. Microbiol.* **2018**, *3* (1), 26–31. https://doi.org/10.1038/s41564-017-0050-1.
(75) Bachmann, V.; Kostiuk, B.; Unterweger, D.; Diaz-Satizabal, L.; Ogg, S.; Pukatzki, S. Bile Salts Modulate the Mucin-Activated Type VI Secretion System of Pandemic Vibrio Cholerae. *PLoS Negl. Trop. Dis.* **2015**, *9* (8), e0004031. https://doi.org/10.1371/journal.pntd.0004031.
(76) MacIntyre, D. L.; Miyata, S. T.; Kitaoka, M.; Pukatzki, S. The Vibrio Cholerae Type VI Secretion System Displays Antimicrobial Properties. *Proc. Natl. Acad. Sci. U. S. A.* **2010**, *107* (45), 19520–19524. https://doi.org/10.1073/pnas.1012931107.
(77) Winans, J. B.; Wucher, B. R.; Nadell, C. D. Cell Group Architecture Dictates Phage Exposure in Multispecies Biofilms. bioRxiv July 25, 2022, p 2022.07.22.501138. https://doi.org/10.1101/2022.07.22.501138.

(78) Hartmann, R.; Singh, P. K.; Pearce, P.; Mok, R.; Song, B.; Díaz-Pascual, F.; Dunkel, J.; Drescher, K. Emergence of Three-Dimensional Order and Structure in Growing Biofilms. *Nat. Phys.* **2019**, *15* (3), 251–256. https://doi.org/10.1038/s41567-018-0356-9.
(79) Parsek, M. R.; Greenberg, E. P. Sociomicrobiology: The Connections between Quorum Sensing and Biofilms. *Trends Microbiol.* **2005**, *13* (1), 27–33. https://doi.org/10.1016/j.tim.2004.11.007.
(80) Mitri, S.; Clarke, E.; Foster, K. R. Resource Limitation Drives Spatial Organization in Microbial Groups. *ISME J.* **2016**, *10* (6), 1471–1482. https://doi.org/10.1038/ismej.2015.208.
(81) Ghoul, M.; Mitri, S. The Ecology and Evolution of Microbial Competition. *Trends Microbiol.* **2016**, *24* (10), 833–845. https://doi.org/10.1016/j.tim.2016.06.011.
(82) Piccardi, P.; Vessman, B.; Mitri, S. Toxicity Drives Facilitation between 4 Bacterial Species. *Proc. Natl. Acad. Sci.* **2019**, *116* (32), 15979–15984. https://doi.org/10.1073/pnas.1906172116.
(83) Coyte, K. Z.; Schluter, J.; Foster, K. R. The Ecology of the Microbiome: Networks, Competition, and Stability. *Science* **2015**, *350* (6261), 663–666. https://doi.org/10.1126/science.aad2602.
(84) Darch, S. E.; West, S. A.; Winzer, K.; Diggle, S. P. Density-Dependent Fitness Benefits in Quorum-Sensing Bacterial Populations. *Proc. Natl. Acad. Sci.* **2012**, *109* (21), 8259–8263. https://doi.org/10.1073/pnas.1118131109.
(85) Stacy, A.; McNally, L.; Darch, S. E.; Brown, S. P.; Whiteley, M. The Biogeography of Polymicrobial Infection. *Nat. Rev. Microbiol.* **2016**, *14* (2), 93–105. https://doi.org/10.1038/nrmicro.2015.8.
(86) Kurkjian, H. M.; Akbari, M. J.; Momeni, B. The Impact of Interactions on Invasion and Colonization Resistance in Microbial Communities. *PLOS Comput. Biol.* **2021**, *17* (1), e1008643. https://doi.org/10.1371/journal.pcbi.1008643.
(87) Momeni, B.; Waite, A. J.; Shou, W. Spatial Self-Organization Favors Heterotypic Cooperation over Cheating. *eLife* **2013**, *2*, e00960. https://doi.org/10.7554/eLife.00960.
(88) Widder, S.; Allen, R. J.; Pfeiffer, T.; Curtis, T. P.; Wiuf, C.; Sloan, W. T.; Cordero, O. X.; Brown, S. P.; Momeni, B.; Shou, W.; Kettle, H.; Flint, H. J.; Haas, A. F.; Laroche, B.; Kreft, J.-U.; Rainey, P. B.; Freilich, S.; Schuster, S.; Milferstedt, K.; van der Meer, J. R.; Groβkopf, T.; Huisman, J.; Free, A.; Picioreanu, C.; Quince, C.; Klapper, I.; Labarthe, S.; Smets, B. F.; Wang, H.; Soyer, O. S. Challenges in Microbial Ecology: Building Predictive Understanding of Community Function and Dynamics. *ISME J.* **2016**, *10* (11), 2557–2568. https://doi.org/10.1038/ismej.2016.45.
(89) Ebrahimi, A.; Schwartzman, J.; Cordero, O. X. Cooperation and Spatial Self-Organization Determine Rate and Efficiency of Particulate Organic Matter Degradation in Marine Bacteria. *Proc. Natl. Acad. Sci.* **2019**, *116* (46), 23309–23316. https://doi.org/10.1073/pnas.1908512116.
(90) Schwartzman, J. A.; Ebrahimi, A.; Chadwick, G.; Sato, Y.; Orphan, V.; Cordero, O. X. Bacterial Growth in Multicellular Aggregates Leads to the Emergence of Complex Lifecycles. bioRxiv November 1, 2021, p 2021.11.01.466752. https://doi.org/10.1101/2021.11.01.466752.
(91) van Gestel, J.; Weissing, F. J.; Kuipers, O. P.; Kovács, Á. T. Density of Founder Cells Affects Spatial Pattern Formation and Cooperation in Bacillus Subtilis Biofilms. *ISME J.* **2014**, *8* (10), 2069–2079. https://doi.org/10.1038/ismej.2014.52.
(92) Dragoš, A.; Kiesewalter, H.; Martin, M.; Hsu, C.-Y.; Hartmann, R.; Wechsler, T.; Eriksen, C.; Brix, S.; Drescher, K.; Stanley-Wall, N.; Kümmerli, R.; Kovács, Á. T. Division of Labor during Biofilm Matrix Production. *Curr. Biol.* **2018**, *28* (12), 1903-1913.e5. https://doi.org/10.1016/j.cub.2018.04.046.
(93) Jautzus, T.; van Gestel, J.; Kovács, Á. T. Complex Extracellular Biology Drives Surface Competition during Colony Expansion in Bacillus Subtilis. *ISME J.* **2022**, 1–9. https://doi.org/10.1038/s41396-022-01279-8.
(94) Damore, J. A.; Gore, J. Understanding Microbial Cooperation. *J. Theor. Biol.* **2012**, *299*, 31–41. https://doi.org/10.1016/j.jtbi.2011.03.008.
(95) Nadell, C. D.; Drescher, K.; Foster, K. R. Spatial Structure, Cooperation and Competition in Biofilms. *Nat. Rev. Microbiol.* **2016**, *14* (9), 589–600. https://doi.org/10.1038/nrmicro.2016.84.
(96) Tan, C. H.; Lee, K. W. K.; Burmølle, M.; Kjelleberg, S.; Rice, S. A. All Together Now: Experimental Multispecies Biofilm Model Systems. *Environ. Microbiol.* **2017**, *19* (1), 42–53. https://doi.org/10.1111/1462-2920.13594.

(97) Røder, H. L.; Olsen, N. M. C.; Whiteley, M.; Burmølle, M. Unravelling Interspecies Interactions across Heterogeneities in Complex Biofilm Communities. *Environ. Microbiol.* **2020**, *22* (1), 5–16. https://doi.org/10.1111/1462-2920.14834.
(98) Enke, T. N.; Leventhal, G. E.; Metzger, M.; Saavedra, J. T.; Cordero, O. X. Microscale Ecology Regulates Particulate Organic Matter Turnover in Model Marine Microbial Communities. *Nat. Commun.* **2018**, *9* (1), 2743. https://doi.org/10.1038/s41467-018-05159-8.
(99) Wolfe, B. E.; Button, J. E.; Santarelli, M.; Dutton, R. J. Cheese Rind Communities Provide Tractable Systems for In Situ and In Vitro Studies of Microbial Diversity. *Cell* **2014**, *158* (2), 422–433. https://doi.org/10.1016/j.cell.2014.05.041.
(100) Huws, S. A.; McBain, A. J.; Gilbert, P. Protozoan Grazing and Its Impact upon Population Dynamics in Biofilm Communities. *J. Appl. Microbiol.* **2005**, *98* (1), 238–244. https://doi.org/10.1111/j.1365-2672.2004.02449.x.
(101) Krause, J.; Ruxton, G. D. *Living in Groups*; OUP Oxford, 2002.
(102) Chesson, P.; Kuang, J. J. The Interaction between Predation and Competition. *Nature* **2008**, *456* (7219), 235–238. https://doi.org/10.1038/nature07248.
(103) Hamilton, W. D. Geometry for the Selfish Herd. *J. Theor. Biol.* **1971**, *31* (2), 295–311. https://doi.org/10.1016/0022-5193(71)90189-5.
(104) *Zebra reduce predation risk in mixed-species herds by eavesdropping on cues from giraffe | Behavioral Ecology | Oxford Academic*. https://academic.oup.com/beheco/article/27/4/1073/1743727 (accessed 2022-07-21).
(105) Weibel, D. B.; Diluzio, W. R.; Whitesides, G. M. Microfabrication Meets Microbiology. *Nat. Rev. Microbiol.* **2007**, *5* (3), 209–218. https://doi.org/10.1038/nrmicro1616.
(106) Sia, S. K.; Whitesides, G. M. Microfluidic Devices Fabricated in Poly(Dimethylsiloxane) for Biological Studies. *ELECTROPHORESIS* **2003**, *24* (21), 3563–3576. https://doi.org/10.1002/elps.200305584.
(107) Hartmann, R.; Jeckel, H.; Jelli, E.; Singh, P. K.; Vaidya, S.; Bayer, M.; Rode, D. K. H.; Vidakovic, L.; Díaz-Pascual, F.; Fong, J. C. N.; Dragoš, A.; Lamprecht, O.; Thöming, J. G.; Netter, N.; Häussler, S.; Nadell, C. D.; Sourjik, V.; Kovács, Á. T.; Yildiz, F. H.; Drescher, K. Quantitative Image Analysis of Microbial Communities with BiofilmQ. *Nat. Microbiol.* **2021**, *6* (2), 151–156. https://doi.org/10.1038/s41564-020-00817-4.
(108) Wucher, B. R.; Bartlett, T. M.; Hoyos, M.; Papenfort, K.; Persat, A.; Nadell, C. D. Vibrio Cholerae Filamentation Promotes Chitin Surface Attachment at the Expense of Competition in Biofilms. *Proc. Natl. Acad. Sci.* **2019**, *116* (28), 14216–14221. https://doi.org/10.1073/pnas.1819016116.
(109) Mukherjee, S.; Brothers, K. M.; Shanks, R. M. Q.; Kadouri, D. E. Visualizing Bdellovibrio Bacteriovorus by Using the TdTomato Fluorescent Protein. *Appl. Environ. Microbiol.* **2016**, *82* (6), 1653–1661. https://doi.org/10.1128/AEM.03611-15.
(110) Hartmann, R.; Jeckel, H.; Jelli, E.; Singh, P. K.; Vaidya, S.; Bayer, M.; Rode, D. K. H.; Vidakovic, L.; Díaz-Pascual, F.; Fong, J. C. N.; Dragoš, A.; Lamprecht, O.; Thöming, J. G.; Netter, N.; Häussler, S.; Nadell, C. D.; Sourjik, V.; Kovács, Á. T.; Yildiz, F. H.; Drescher, K. Quantitative Image Analysis of Microbial Communities with BiofilmQ. *Nat. Microbiol.* **2021**, *6* (2), 151–156. https://doi.org/10.1038/s41564-020-00817-4.

Figures

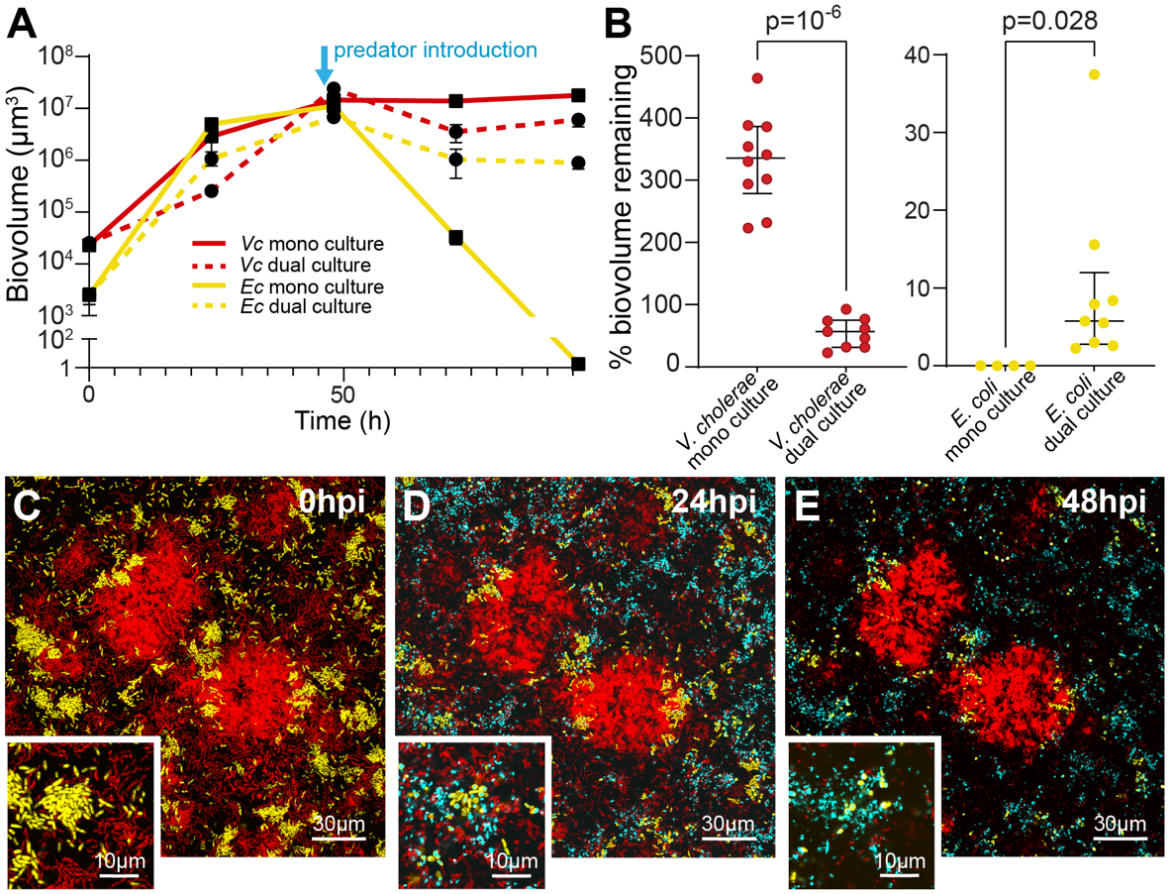

740 **Figure 1.** Population dynamics in mono culture and dual culture biofilms of *V. cholerae* and *E. coli* undergoing predation by *B. bacteriovorus*. Biofilms of *V. cholerae* (red) and *E. coli* (yellow) were grown for 48h prior to *B. bacteriovorus* (cyan) predator exposure. (A) population dynamics of each prey species in monoculture and dual culture biofilm growth (n = 4). (B) Percent change in prey biovolume, a direct proxy for population size, 48h after predator introduction relative to just prior to predator introduction, both
745 in single species prey biofilm controls and dual species prey co-culture biofilm conditions. (*V. cholerae* monoculture n = 10; *V. cholerae* dual culture n = 9; *E. coli* monoculture n = 4; *E. coli* dual culture n = 9. Pairwise comparisons were performed with Mann-Whitney U-tests. (C-E) Representative images of dual culture biofilms at (C) 48h after initial prey inoculation (just prior to predator introduction; 'hpi' denotes 'hours post introduction' of predators), (D) 24h post introduction of predators, and (E) 48h post introduction
750 of predators. Inset frames show regions with details of predators entering host cells and forming rounded bdelloplasts, indicating active predation.

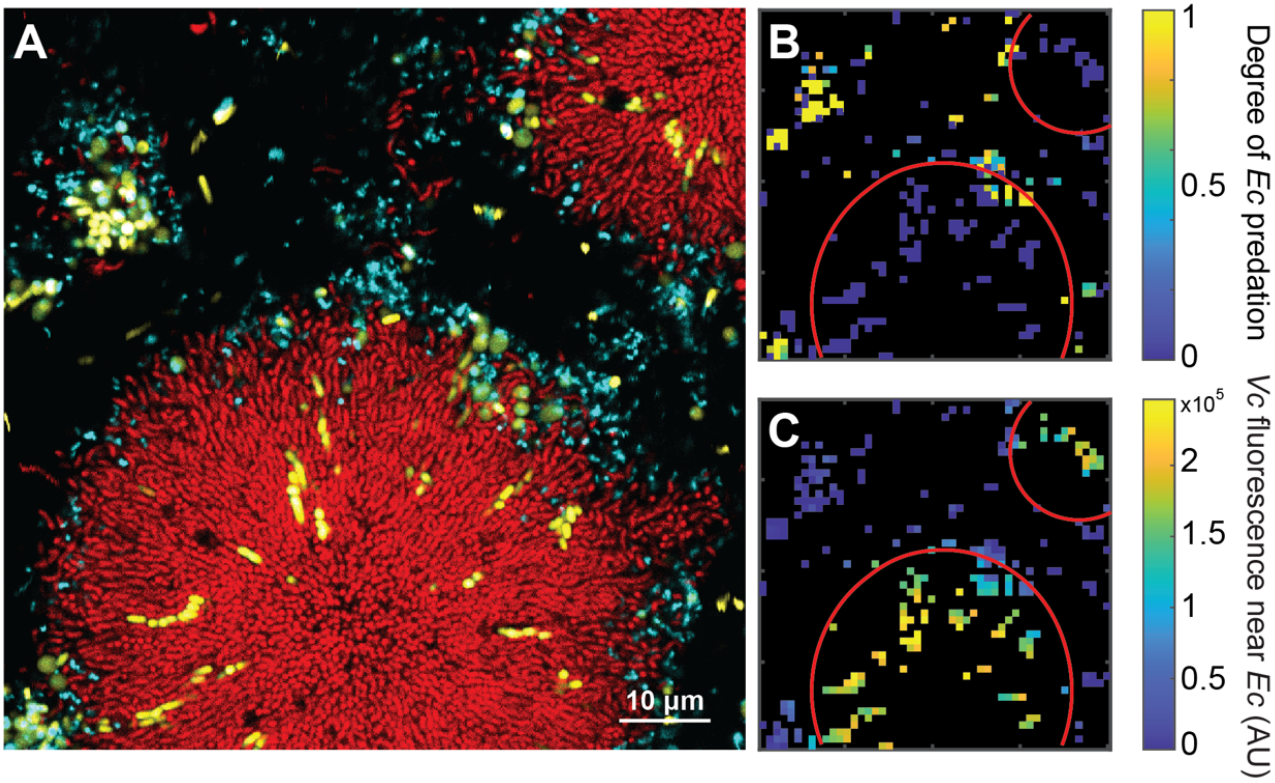

Figure 2. *E. coli* enveloped within highly packed *V. cholerae* biofilms can be protected from *B. bacteriovorus* exposure. (A) Representative image demonstrating the ability of highly packed *V. cholerae* biofilms (red) to protect *E. coli* biomass (yellow) from access by *B. bacteriovorus* (cyan). (B) Heatmap of the degree of predation on *E. coli*, quantifying raw data from panel A. Red circles denote boundaries of highly packed *V. cholerae* cell groups. (C) Heatmap of *V. cholerae* fluorescence within 5µm of each unit of segmented biovolume of *E. coli* from panel A.

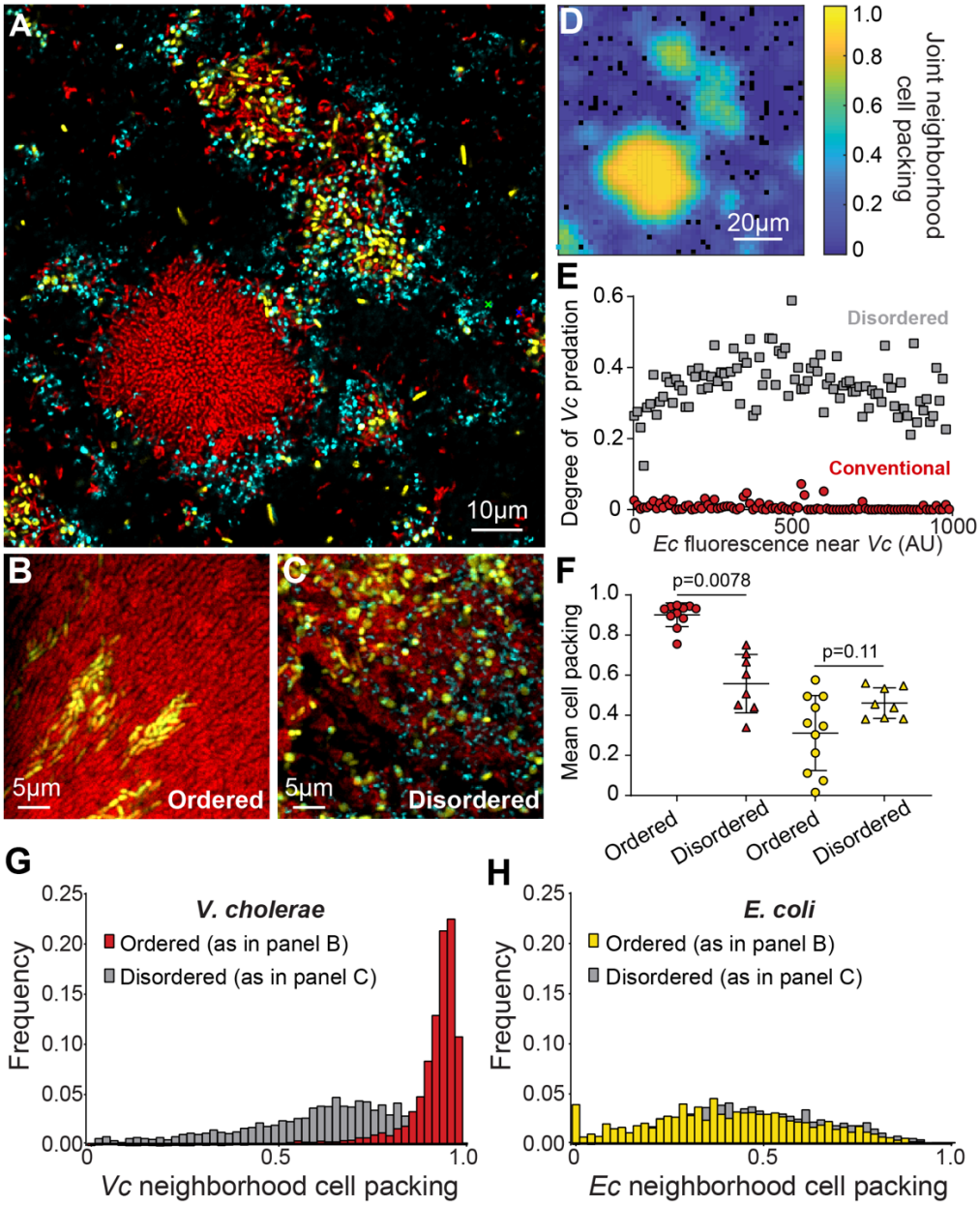

Figure 3. *V. cholerae* and *E. coli* exhibit two distinct joint biofilm morphologies in co-culture that strongly affect *B. bacteriovorus* predation susceptibility. (A) Representative image of both biofilm dual species cell group types, which can occur in close proximity. The structure we term 'ordered' more closely resembles the architecture *V. cholerae* produces on its own and is shown on the lower left in this image. The novel, well-mixed structure, which we term 'disordered', is shown on the upper right. (B-C) Additional higher magnification images detailing the architecture of ordered and disordered colony morphologies. (D) Heatmap of the combined two species neighborhood cell packing values for the image in panel A. (E) Scatterplot of the degree of predation on *V. cholerae* as a function of the fluorescence of *E.coli* in proximity to *V. cholerae* biomass. The data are split according to whether they are from ordered architecture colonies (n = 11), or disordered colonies (n = 9). (F) Mean within-species cell packing for *V. cholerae* (red) and *E. coli* (yellow) in cell groups of each structure type (ordered n = 11; disordered n = 9). Pairwise comparisons were performed by Mann-Whitney U-test. (G-H) Full frequency distributions of within-species cell packing for (G) *V. cholerae* and (H) *E. coli* within each cell group type.

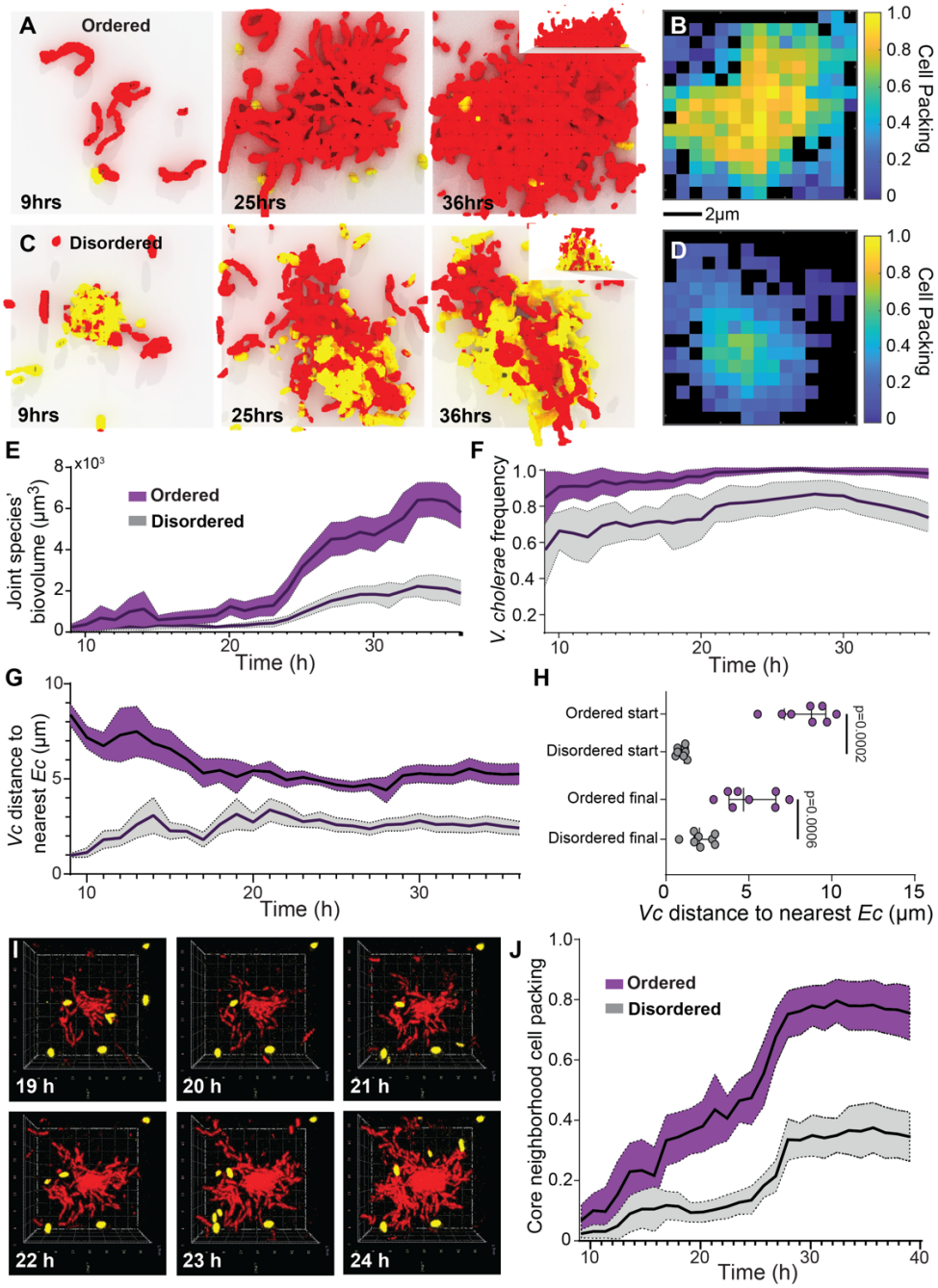

Figure 4. The initial distance between *V. cholerae* and *E. coli* cells best distinguishes colonies that will become highly packed and predation-protected versus disordered and predation-susceptible. (A) Time lapse of 3D renderings of an example ordered cell group with (B) a heatmap for neighborhood cell packing at the 36h time point. (C) Time lapse of 3D renderings of an example disordered cell group with (D) a heatmap for neighborhood cell packing at the 36h time point. Renderings in panels A and C are 31μm x 31μm x 14μm) (LxWxD). (E-G) Time courses for (E) combined biovolume of both species, (F) *V. cholerae* frequency, (G) Average distance of *V. cholerae* cells to nearest *E. coli* (n = 8 for each colony type). (H) Statistical comparison of *V. cholerae* distance to nearest *E. coli* between biofilm types at the start and end of courses in G (Mann-Whitney U tests with n =8). (I) Top-down view of a *V. cholerae* cluster as a core high-packing region nucleates (each rendering is 31μm x 31μm x 14μm) (LxWxD). (J) Time courses of neighborhood cell packing in the core regions (within 10μm of colony center) of both colony types.

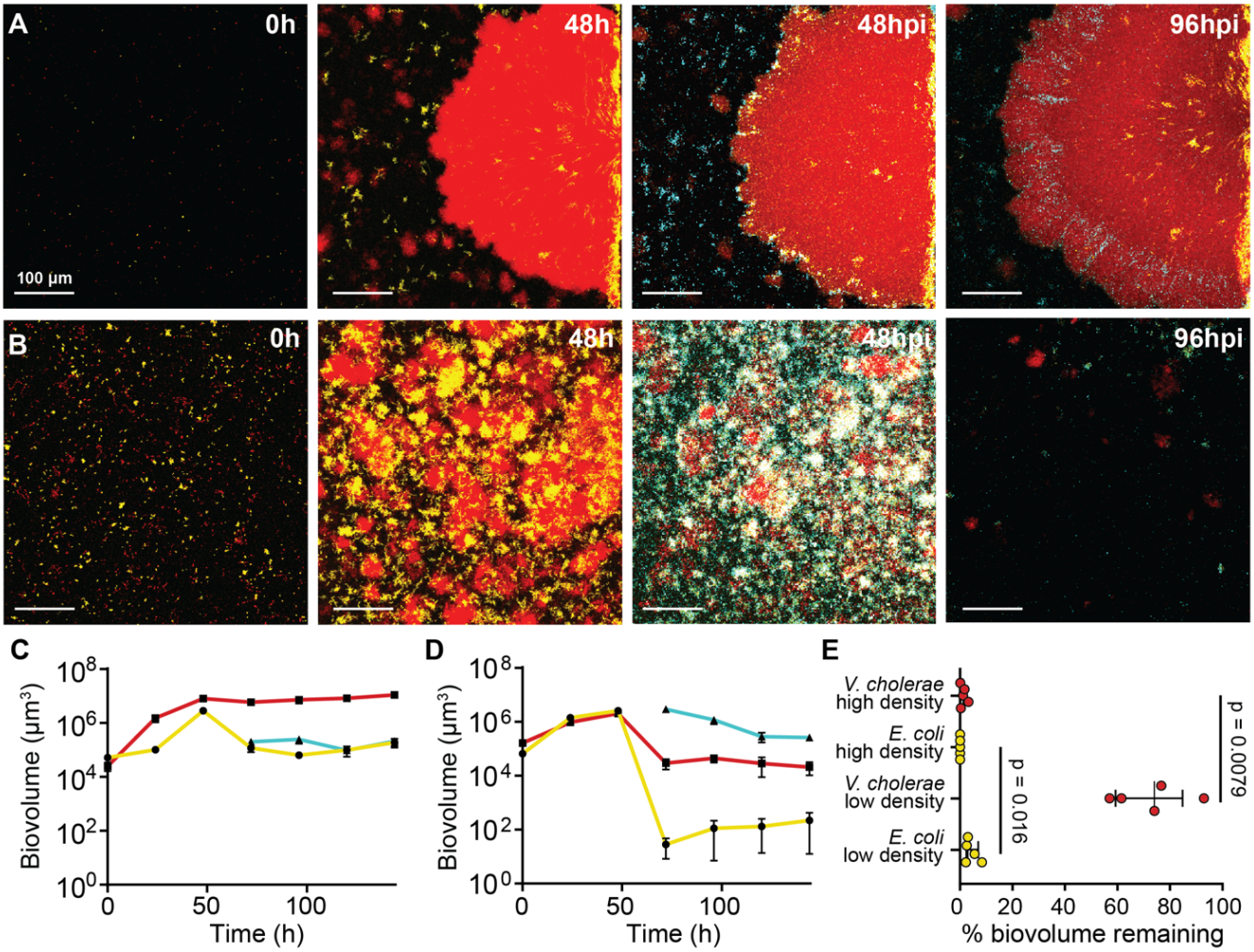

Figure 5. Initial surface colonization density alters the fraction of highly packed versus disordered colonies of *E. coli* and *V. cholerae*, which in turn alters overall population dynamics and predator survival for both prey. (A,B) Representative image sets of the low density (A) and high density (B) colonization conditions at initial surface colonization through 96 hours post predator introduction. (C,D) Biovolume of all three species as a proxy for their population dynamics in the (C) low-density initial condition and (D) high-density arena ($n = 4$). (E) Per cent of each prey species remaining at the end of the predation experiments in the low and high colonization density initial conditions ($n = 5$). Pairwise comparisons are Mann-Whitney U tests with Bonferroni correction.

Supplemental Information

Breakdown of cooperative architecture in multispecies biofilms and the spatial ecology of predation

Benjamin R. Wucher[1], Mennat Elsayed[2], Daniel E. Kadouri[2], Carey D. Nadell[1]*

[1] Department of Biological Sciences, Dartmouth, 78 College St., Hanover, NH 03755, USA
[2] Department of Oral Biology, Rutgers School of Dental Medicine, 110 Bergen St., Newark, NJ 07101, USA

*Author for correspondence:
Carey D. Nadell (ORCID: 0000-0003-1751-4895)
1978 Life Sciences Center
78 College St., Hanover NH 03755
Email: carey.d.nadell@dartmouth.edu
Phone: 603-646-1525

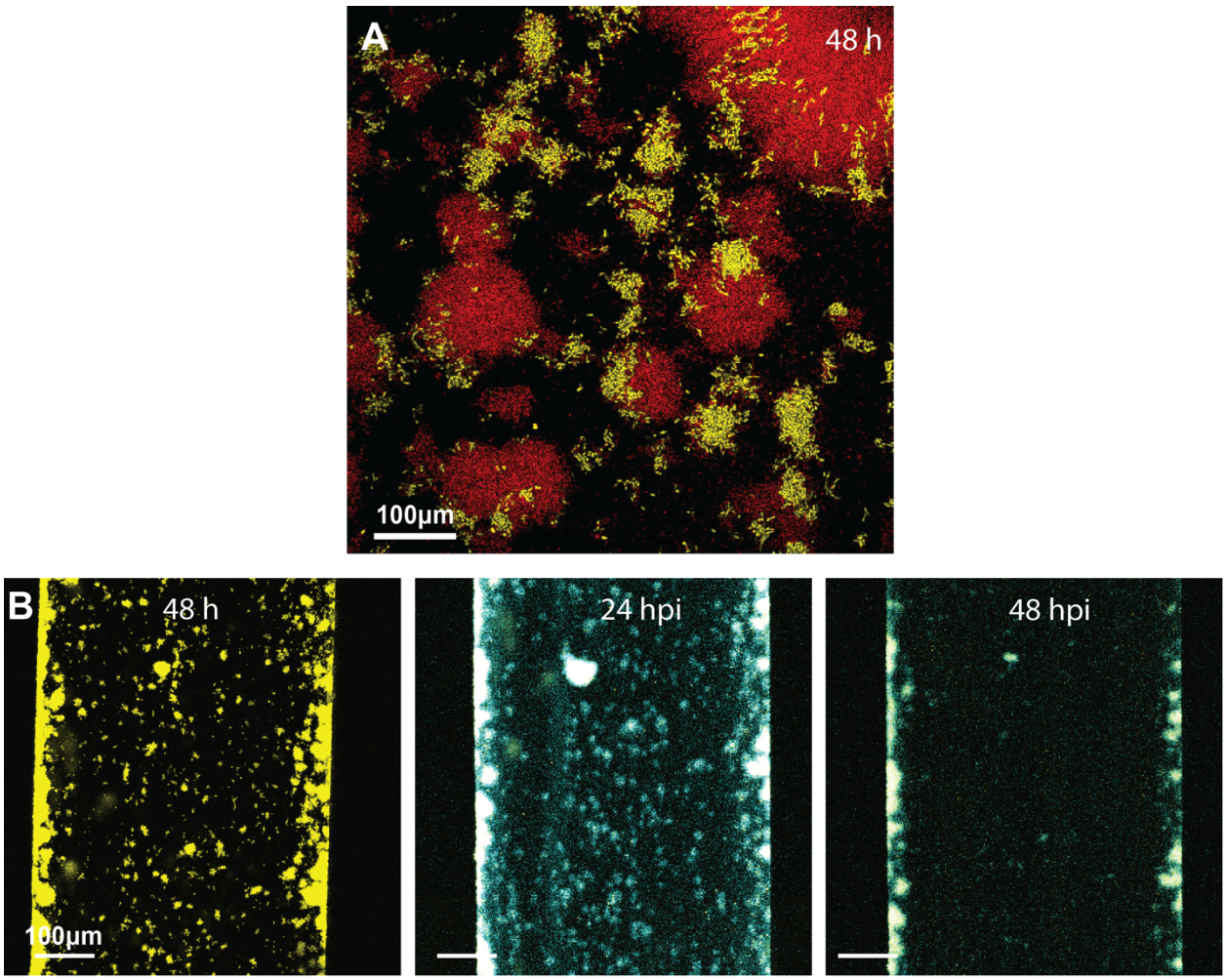

Figure S1. (A) Image of cohabitation of *E. coli* and *V. cholerae* and variable colony structure in microfluidic culture conditions. (B) *E. coli* mono-culture biofilm representative images at 48h of growth and 24, 48 hours post introduction (hpi) of predators. The few remaining *E. coli* cells present at 48 hpi can be seen still undergoing predation by *B. bacteriovorus* and ultimately die as well.

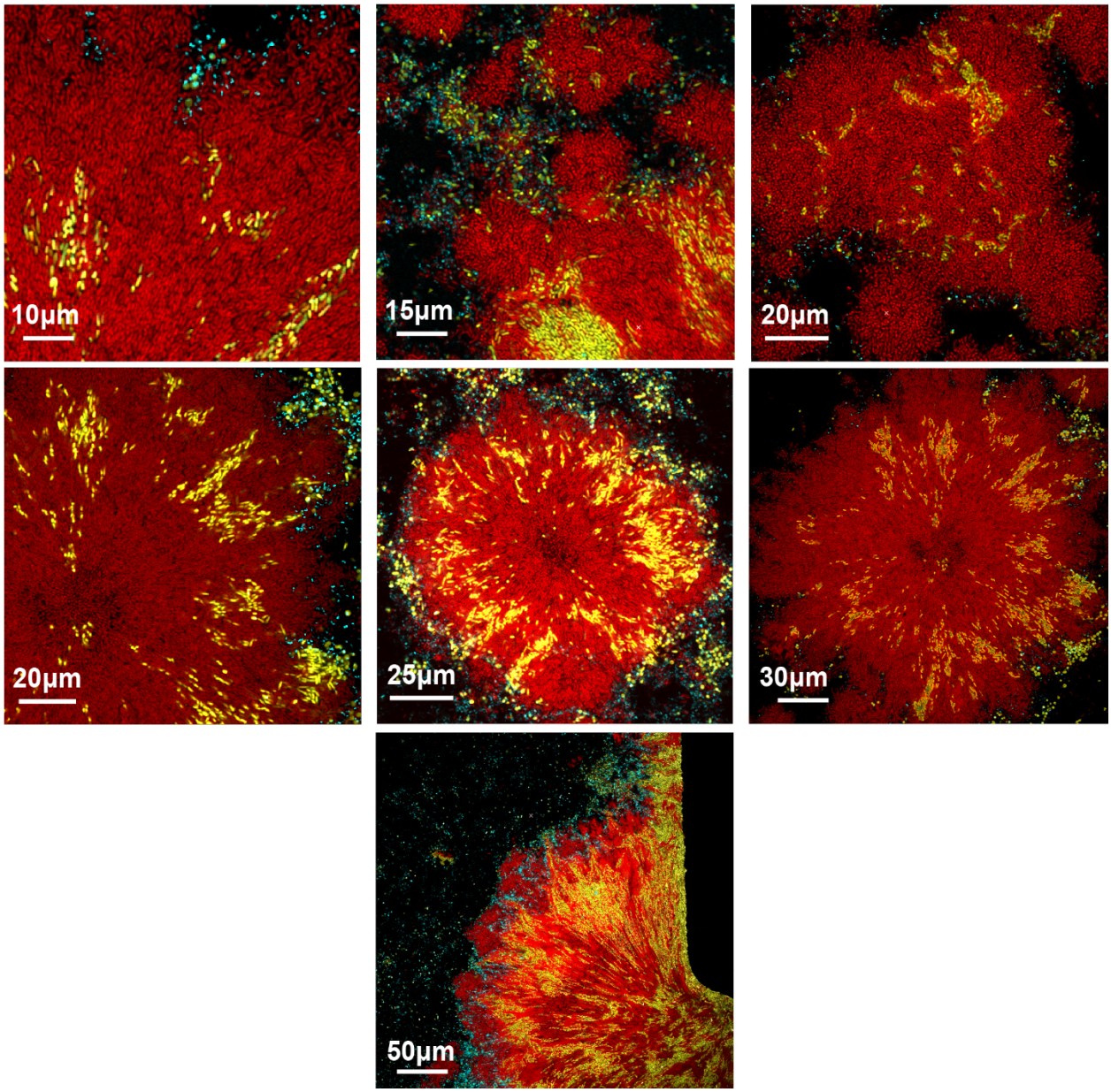

820 **Figure S2. Representative examples of *E. coli* inclusions within conventional *V. cholerae* biofilm structures with high cell packing**

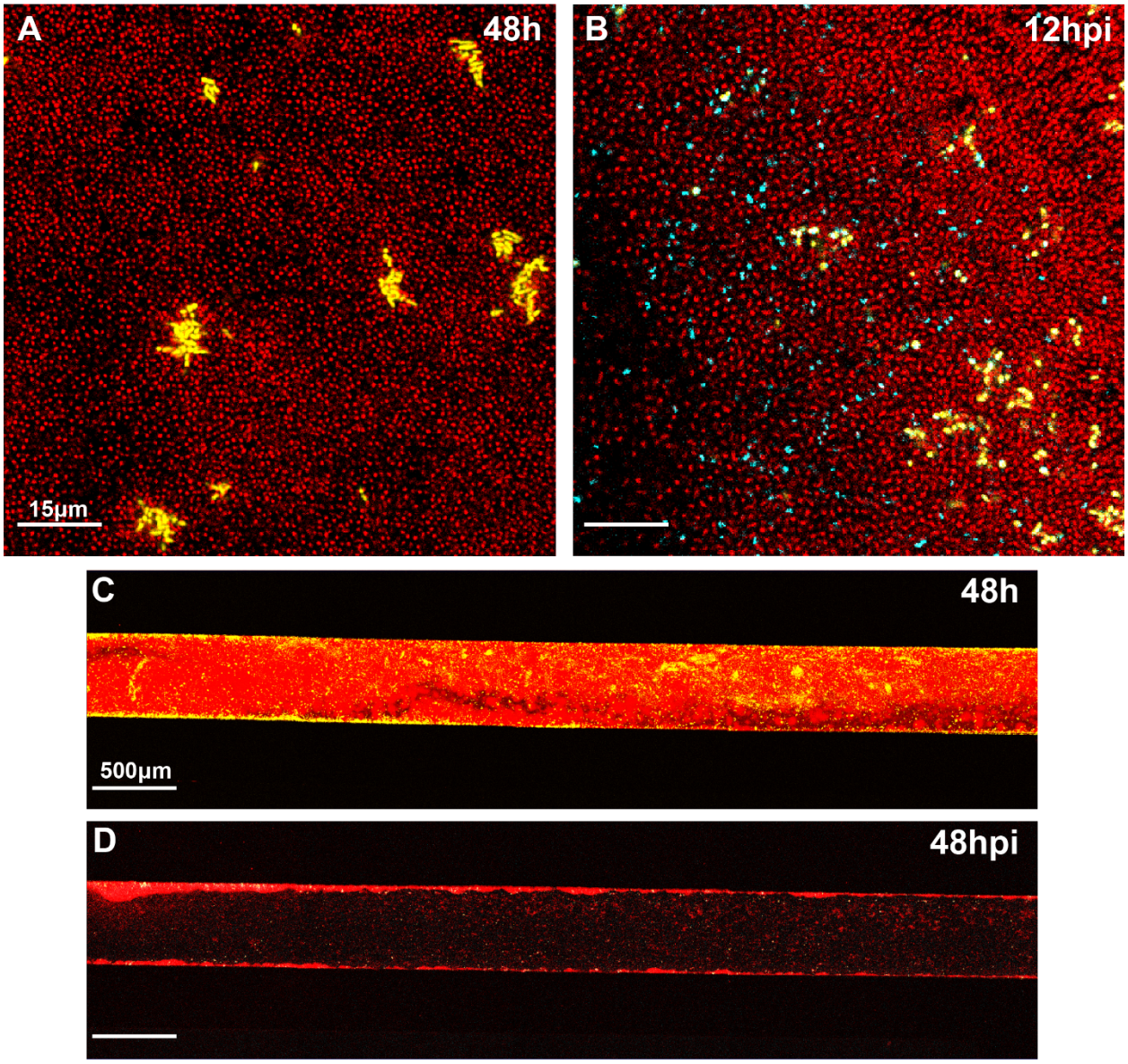

Figure S3. *ΔrbmA V.cholerae* biofilms cannot protect *E. coli* inclusions from bacterial predation. (A-B) *E. coli* and *ΔrbmA* biofilm growth at 48h and 48h after predator introduction. (C-D) Whole microfluidic chamber images showing *E. coli* and *ΔrbmA V. cholerae* biofilm growth (C) before and (D) after predation.

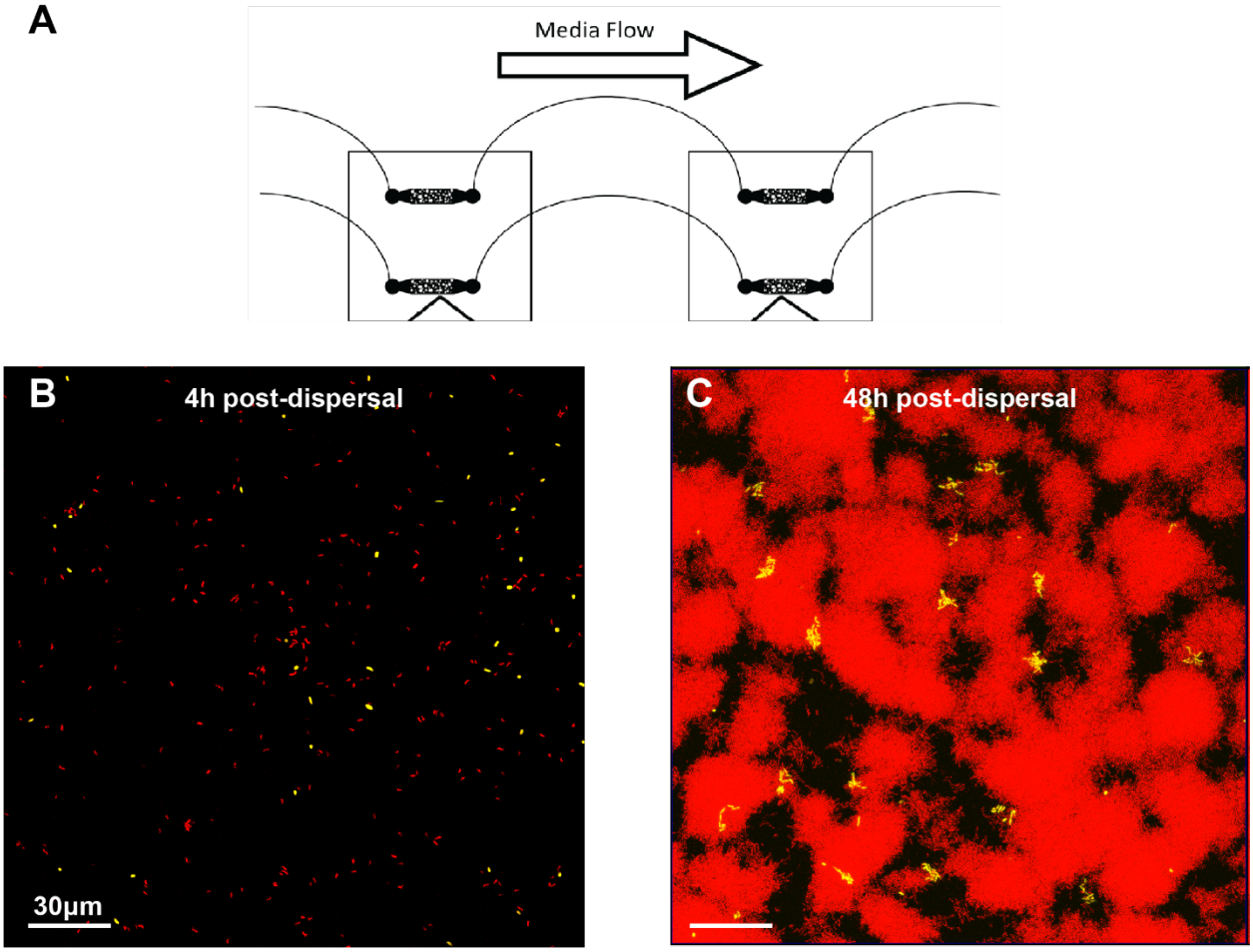

Figure S4. Dispersal of dual species biofilms post predation shows that *E. coli* growing within mature *V. cholerae* colonies remain viable and can disperse to downstream locations. (A) Schematic of "daisy chain" of microfluidic devices used to introduce dispersing cells to new colonization environment. (B) Both species successfully attach to the surface of the new microfluidic chamber after dispersal. (C) Dual species biofilm growth can be seen in the new microfluidic chamber after 48 hours of growth.

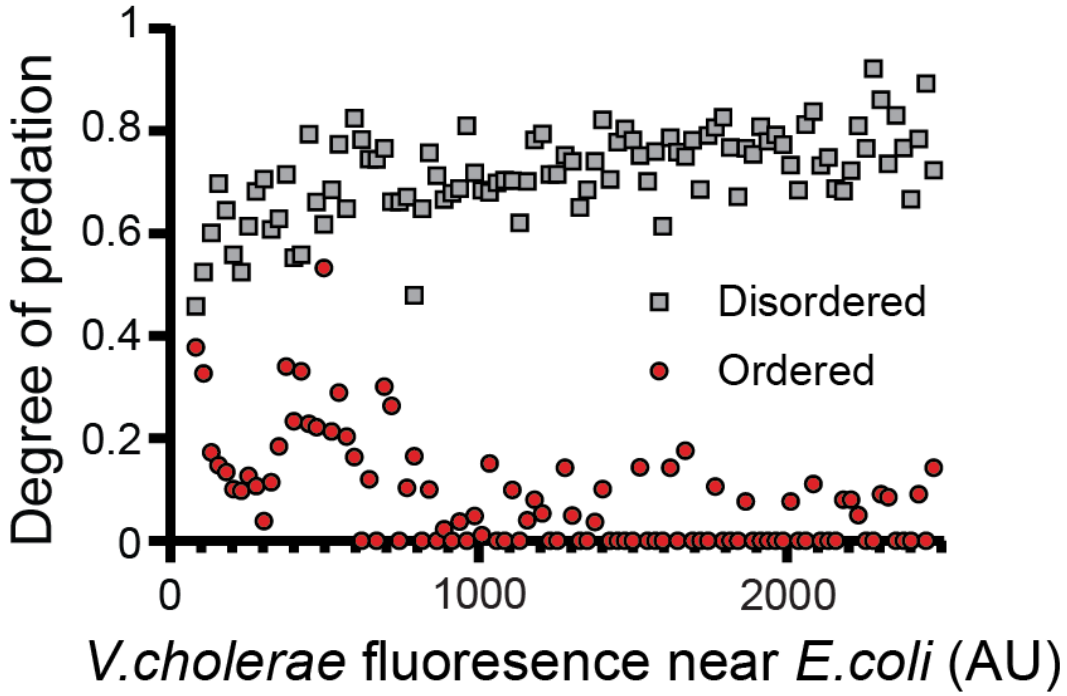

Figure S5. Analysis of *E. coli* predation as a function of *V. cholerae* fluorescence in proximity to *E. coli* biomass, related to main text Figure 3E.

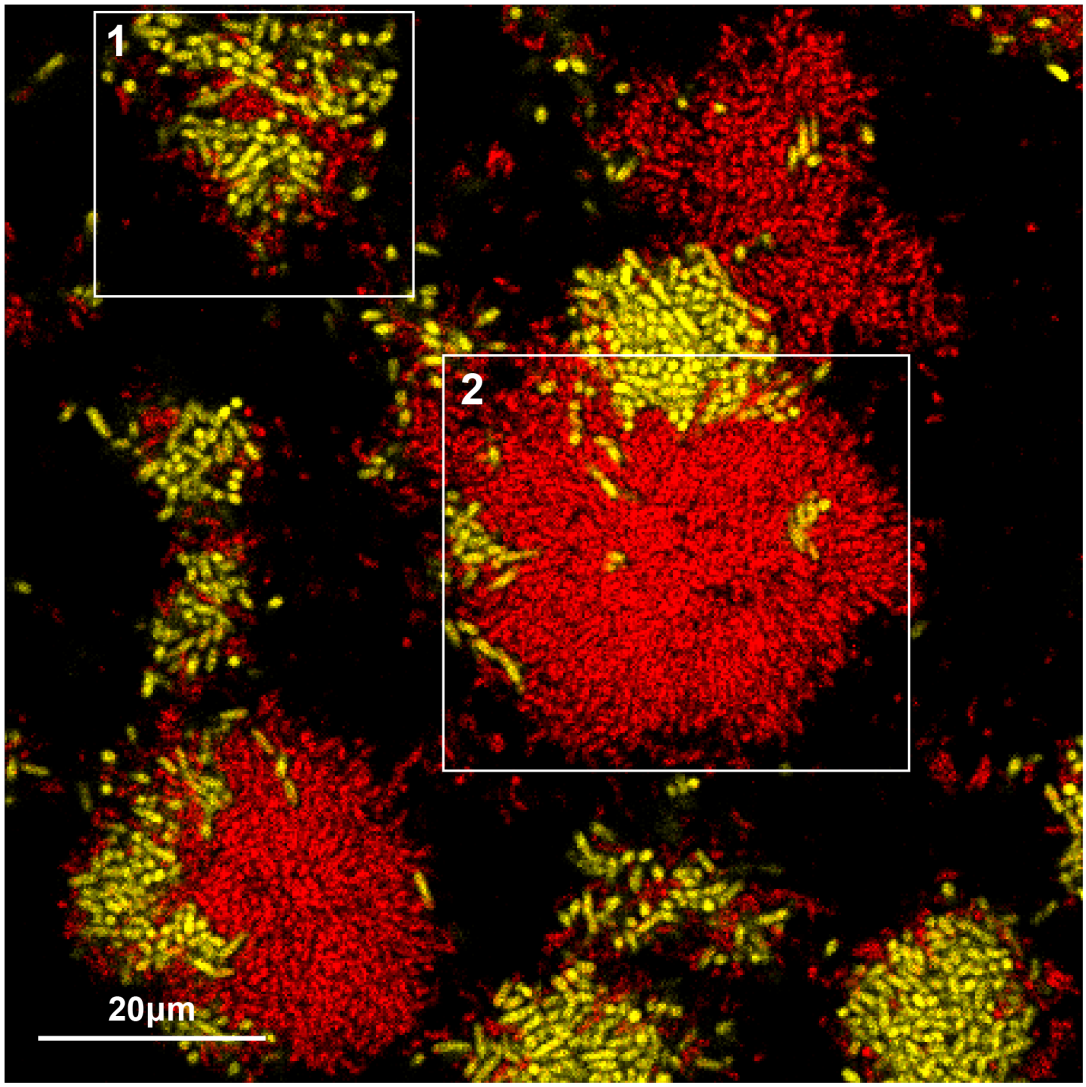

Figure S6. Two different dual species biofilm morphology types containing *V. cholerae* (red) and *E. coli* (yellow) occur within close proximity to one another. (1: Disordered; 2: Ordered)

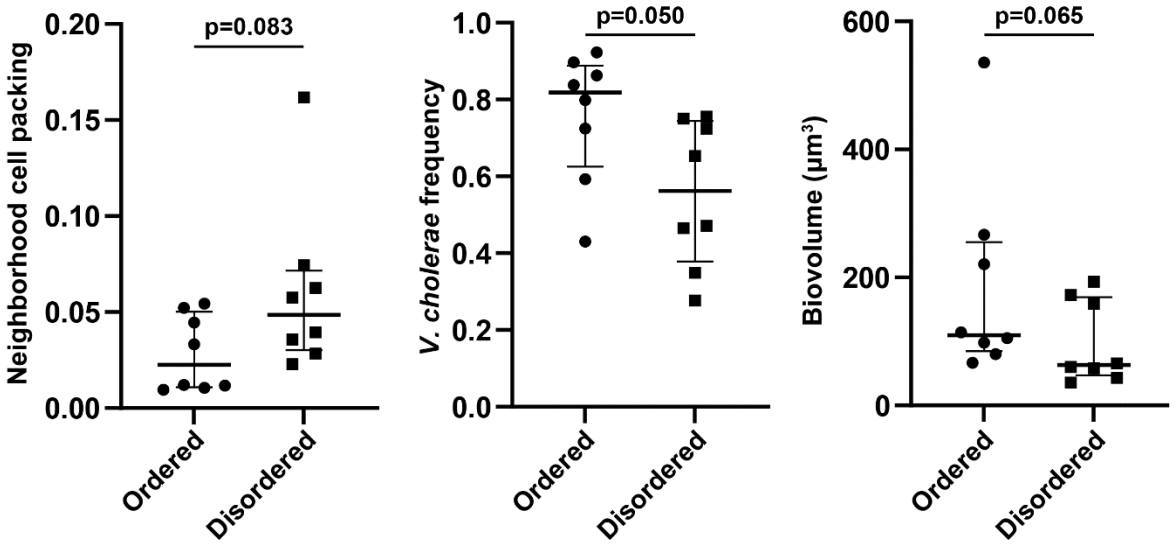

845 **S7. Relative to initial distance between *V. cholerae* and *E. coli* cells (see main text Figure 4G), measures of cell packing, *V. cholerae* relative abundance, and total biovolume at the start of biofilm growth were not significant significantly different between cell groups that would ultimately produce ordered high-packing microcolonies or disordered microcolonies.**

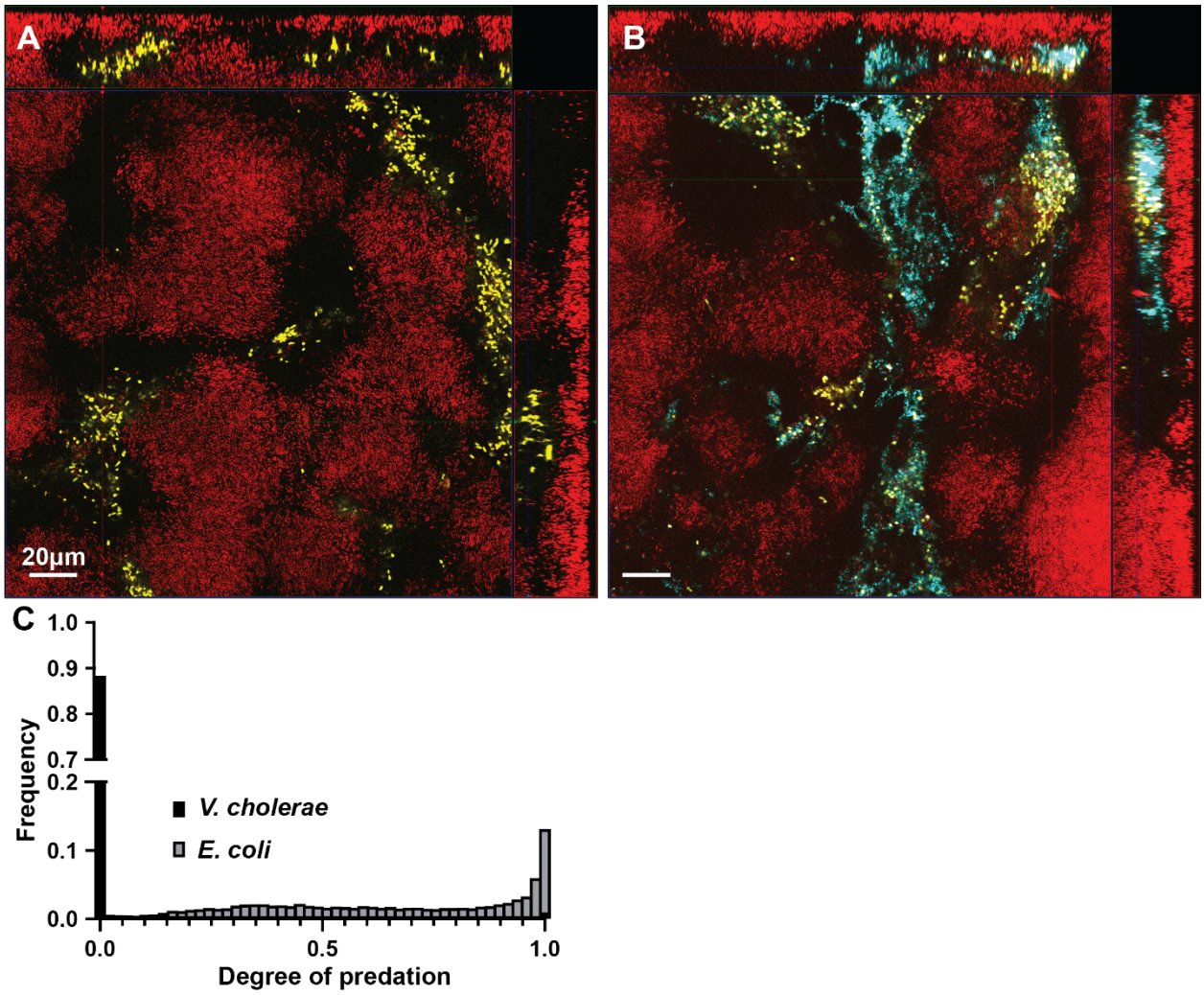

S8 Continuous introduction of *E. coli* after *V. cholerae* biofilm establishment does not change the morphology of *V. cholerae* biofilms. (A/B) representative images of *V. cholerae* biofilms grown for 48 h prior to the continuous introduction of *E. coli* cells in the media, before and 1 h after predator introduction. (C) Frequency distribution of predation for *V. cholerae* and *E. coli* in this experiment.

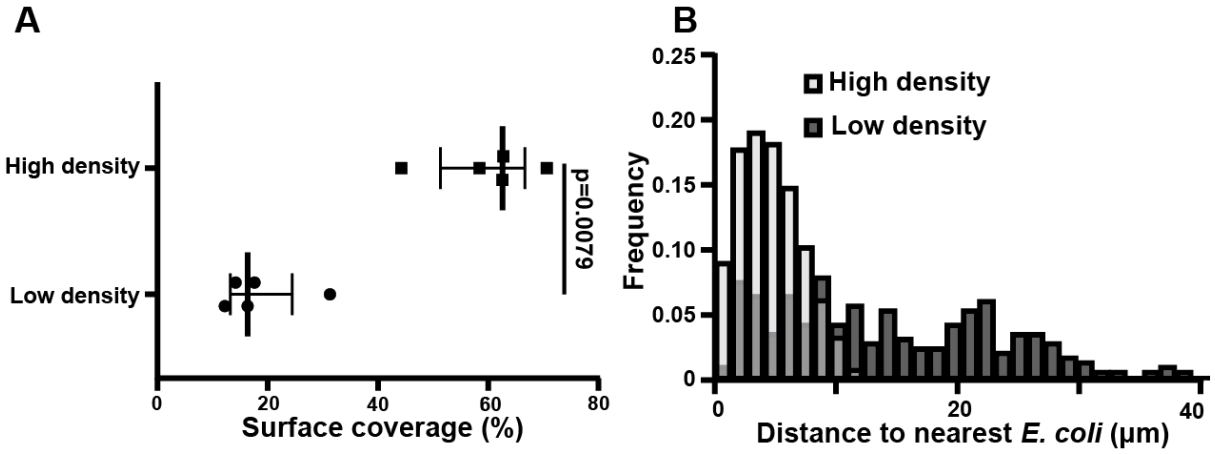

Figure S9. Surface coverage and distributions of distances between *V. cholerae* and *E. coli* in high versus low surface colonization density experiments. (A) Comparison of average surface colonization
865 between high- and low-density arenas. Pairwise comparison by Mann-Whitney U-test. (B) Frequency distribution of the average distance to the nearest *E. coli* cell for all *V. cholerae* in low versus high surface colonization density settings.